Title: Insights into the pathogenesis of ulcerative colitis from a murine model of stasis-induced dysbiosis, colonic metaplasia, and genetic susceptibility

Authors: Marc A. Ward[1*], Joseph F. Pierre[2*], Raquel F. Leal[3], Yong Huang[2], Benjamin Shogan[1], Sushila R. Dalal[2], Christopher R. Weber[4], Vanessa A. Leone[2], Mark W. Musch[2], Gary C. An[1], Mrinalini C. Rao[5], David T. Rubin[2], Laura E. Raffals[7], Dionysios A. Antonopoulos [2,8,9], Mitch L. Sogin[6], Neil H. Hyman[1], John C. Alverdy[1], Eugene B. Chang[2]

Affiliations:
[1]Department of Surgery, University of Chicago, Chicago, IL
[2]Department of Medicine, Knapp Center for Biomedical Discovery, University of Chicago, Chicago, IL
[3]Colorectal Surgery Unit, Department of Surgery, University of Campinas, Campinas, Sao Paulo, Brazil.
[4]Department of Pathology, University of Chicago
[5]Department of Physiology and Biophysics, University of Illinois at Chicago, Chicago, IL
[6]Josephine Bay Paul Center, Biosciences Division, Marine Biological Laboratory at Woods Hole, Woods Hole, MA
[7]Department of Medicine, Mayo Clinic, Rochester, MN
[8]Biosciences Division, Argonne National Laboratory, Argonne, IL
[9]Institute for Genomics and Systems Biology, University of Chicago, Chicago, IL

*These authors made major contributions and contributed equally to the studies.

One sentence Summary: Microbial stasis in small intestinal self-filling blind loops drives mucosal adaptations mimicking colon, leading to inflammatory disease in colitis-susceptible hosts.

Key Words: Pouchitis; Inflammatory Bowel Disease; Ulcerative Coltiis; Dysbiosis

Abbreviations:
IBD, UC, IPAA, SFL, SEL, SPF, PCoA, Wnt-5a, SHH, PDGFRα, PAS, Ki-67

Abstract:

Gut dysbiosis, host genetics, and environmental triggers are implicated as causative factors in inflammatory bowel disease (IBD), yet mechanistic insights are lacking. Longitudinal analysis of ulcerative colitis patients following total colectomy with ileal anal anastomosis (IPAA) where >50% develop pouchitis, offers a unique setting to examine cause vs. effect. To recapitulate human IPAA, we employed a mouse model of surgically created blind self-filling (SFL) and self-emptying (SEL) ileal loops using wild-type (WT), IL-10 KO (IL10), and TLR4 KO (T4), and IL10/T4 double KO mice. After 5 weeks, loop histology, host gene/protein expression, and bacterial 16s rRNA profiles were examined. SFL exhibit fecal stasis due to directional motility oriented towards the loop end, whereas SEL remain empty. In wild type mice, SFL, but not SEL, develop pouch-like microbial communities without accompanying active inflammation. However, in genetically susceptible IL-$10^{-/-}$ deficient mice, SFL, but not SEL, exhibit severe inflammation and mucosal transcriptomes resembling human pouchitis. The inflammation associated with IL-10-/- required TLR4, as animals lacking both pathways displayed little disease. Furthermore, germ-free $IL10^{-/-}$ mice conventionalized with SFL, but not SEL, microbiota populations develop severe colitis. These data support essential roles of stasis-induced, colon-like microbiota, TLR4-mediated colonic metaplasia, and genetic susceptibility in the development of pouchitis and possibly UC. However, these factors by themselves are not sufficient. Similarities between this model and human UC/pouchitis provide opportunities for gaining insights into the mechanistic basis of IBD and for identification of targets for novel preventative and therapeutic interventions.

Introduction: The incidence of inflammatory bowel diseases (IBD) has increased over the last century (16) and over 160 gene variants associated with increased risk for IBD (8, 14) have now been identified. However, genetic risk alone is insufficient to account for most cases of IBD. The development of gut dysbiosis due to non-genetic environmental stressors is now believed to be another important factor in either causing or driving IBD (8). While lifestyle changes, including the use of antibiotics, sanitation, vaccinations, and shifts to 'Westernized' diets, certainly contribute, the underlying etiologies for IBD susceptibility remain unclear. Host intestinal homeostasis is strongly influenced by the microbiome, with the epithelium and underlying lymphoid cells normally sensing colonizing microbes and reciprocally establishing an immunologically tolerant mucosal barrier (24). However, in genetically susceptible hosts, altered microbial diversity can lead to aberrant immunological responses and greater IBD risk. The inability to follow patients from a known "time-zero" until the development of mucosal inflammation makes it difficult to draw conclusions about the roles of specific communities of bacteria in IBD. Most likely, IBD is caused by the convergence of genetic susceptibility and non-genetic environmental stressors that cause intestinal dysbiosis (1, 13, 18), and the underlying mechanisms remain to be elucidated.

Ulcerative colitis (UC) is a clinical subset of IBD characterized by inflammation occurring exclusively in the colon with sparing of the small intestine. In medically refractory UC, occurring in an estimated 30-50% of patients, the ultimate treatment is total proctocolectomy, followed by the surgical creation of an ileal pouch anal anastomosis (IPAA) (1, 6). The terminal ileum is typically configured into a double-limbed pouch and is connected to the anal canal, so as to serve as a reservoir for stool and permit continence of intestinal contents. An initial ileostomy is constructed to allow the IPAA surgery to heal and after 2-3 months; if no abnormalities are detected, the ileostomy is taken down, restoring the fecal flow to the ileal pouch. UC patients, however, are at increased risk of inflammation of the pouch, termed pouchitis, as compared to non-IBD patients (i.e those with familial adenomatous polyposis) who undergo similar surgical pouch construction and rarely, if ever, develop pouchitis (1). While other causative factors continue to be investigated, pouchitis patients exhibit microbial dysbiosis and often respond to antibiotic treatment (5), implicating microbes as causal agents. Since UC-associated disease normally spares the small intestine, understanding the altered microbial community structure and reciprocal mucosal regulation that predisposes the ileal pouches of IPAA to inflammatory complications may provide important clues to our understanding of IBD. Yet model systems have been lacking.

Here, we investigate a clinically relevant murine surgical model of IPAA using wild type (WT) and IL-10 deficient (IL-$10^{-/-}$) mice genetically prone to IBD with self-filling blind ileal loops (SFL), versus self-emptying loops (SEL) as controls. Our results demonstrate a dramatic microbial community restructuring and altered host mucosal and immune regulation as a consequence of intestinal stasis in SFL loops. The necessary role of microbes in disease pathogenesis is underscored by the lack of IBD in germ-free animals. The IL10/TLR4 axis underlies the inflammatory disease in the genetically prone host of this model. Our model defining the essential role for fecal stasis, gut dysbiosis, and genetic susceptibility offers insights into human pouchitis and UC.

Materials and Methods:

Animals and human samples

Human biopsies and stool samples were obtained under IRB approval and all privacy and consent protocols were followed. Human biopsies were taken from ulcerative colitis patients who underwent a total abdominal proctocolectomy with ileal pouch-anal anastomosis at the University of Chicago Medical Center between 2009-2011. Patients provided informed consent, and the institutional review board of the University of Chicago approved the study. UC patients with IPAA underwent sequential endoscopic evaluations of their pouches with biopsies and luminal aspirates. Biopsies were obtained from the pouch base (pouch) as well as the normal ileum proximal to the pouch (pre-pouch). All animal protocols were approved by IACUC at the University of Chicago. Mice (C57Bl/6 background) were originally purchased from Jackson Laboratory (IL-10, Stock# 002250; TLR4, Stock# 007227. Bar Harbor, ME) and bred in-house under standard 12:12 light/dark conditions at the University of Chicago. IL-10 and TLR4 knockouts were maintained as homozygous; Double-knockouts were bred in-house and maintained as homozygous. Female mice, approximately 8 weeks old, were fed *ad libitum* gel diet 76A (Cat# 72-07-5022, Clear H20, Portland, ME) starting 5-days prior to surgery to prevent obstruction at the anastomosis. Females were used because our pilot studies demonstrated better surgical recovery and survival compared with male counterparts. Animals were deeply anesthetized with Ketamine (100 mg/kg) and Xylazine (10 mg/kg) Aseptic surgery was performed to resect 2.5 cm of ileum 3 cm proximal to the ileal-cecal value with anastomosis to the ileum using 8-0 suture (**Figure 1a**). In contrast to human surgery, colons are not removed in our mouse model, since this procedure would dramatically complicate the surgical procedure,

prolong surgical recovery, and decrease animal survival The abdominal wall was closed with interrupted 4-0 silk suture and skin was closed with staples. Analgesics (2 mg/kg buprenorphine) were provided post-operatively. DSS experiments were performed as previously described (3), administering 2% DSS (Cat# 160110, Affymetrix/USB/MP, Cleveland, OH) for 3 days. After 5 weeks, mice were humanely euthanized. Intestinal loops and sham tissues were collected for RNA, protein, and histology. Loop, sham ileum, and sham colon contents were collected and snap frozen at −80°C for microbiota analysis.

RNA extraction, cDNA synthesis, and quantitative real-time PCR

Total RNA isolation was performed on mucosal scrapings with the Trizol (Ambion) and chloroform method. RNA concentration and quality was determined by UV spectrophotometry. RNA was reverse transcribed using anchored-oligo (dT) and random hexamer primers. Following RT (Transcriptor Reverse Transcriptase Reaction buffer 5X; Protector RNase Inhibitor 40U/µl; Deoxynucleotide Mix, 10mM; Transcriptor Reverse Transcriptase 20U/µl; Roche Applied Science, Indianapolis, IN), RT-PCR was performed on resulting cDNA in triplicate, using the manufacturer's protocol (Roche Applied Science), in LightCycler® capillary. Gene-specific primers from murine GAPDH, PDGFRα, SHH, Wnt5a, IFNγ, TNFα, IL-1β, TLR2, and TLR4, in addition to human GAPDH, Wnt-5a, and PDGFRα are shown in **Table 5**. The optimal concentration of cDNA and primers, as well as the maximum efficiency of amplification, were obtained through five-point, two-fold dilution curve analysis for each gene. RT-PCR amplification consisted of an initial denaturation step (95°C for 10 min), 45 cycles of denaturation (95°C for 10s), annealing (55°C for 20s) and extension (60°C for 30s), followed by a final incubation at 55°C for 30s and cooling at 40°C for 30s. All measurements were normalized by the expression of GAPDH gene, considered as a stable housekeeping gene. Gene expression was determined using the delta-delta Ct method: $2^{-\blacktriangle\blacktriangle CT}$($\blacktriangle\blacktriangle$CT=[Ct(target gene) – Ct(GAPDH)]$_{patient}$ – [Ct(target gene) – Ct(GAPDH)]$_{control}$). Real-time data were analyzed using the Roche LightCycle® (Roche Applied Science).

DNA isolation

Intestinal contents were homogenized in 1 ml extraction buffer [50mM Tris (pH 7.4), 100mM EDTA (pH 8.0), 400mM NaCl, 0.5% SDS] containing 20uL proteinase K (20 mg/ml, Cat# 03115887001, Roche). 0.1-mm-diameter zirconia/silica beads (BioSpec Products, Bartlesville, OK, USA) were added to the extraction tubes and a Mini-Beadbeater-8 cell disrupter (BioSpec Products) for 5 minutes to lyse cells. After overnight incubation at 55°C with

agitation, extraction with phenol:chloroform:isoamyl alcohol, and precipitation with ethanol were performed. Isolated DNA was dissolved in nuclease-free water and stored at −80°C.

16S rRNA-based Polymerase Chain Reaction, Illumina Library Preparation, and Data Analysis

Polymerase chain reaction was performed as follows: 5μL of 10x Ex Taq buffer containing 20mM $MgCl_2$ (Takara, Tokyo, Japan), 4μL of 2.5mM dNTP Mixture (Takara), 1μL each of forward (27F, 5′-AGA GTT TGA TCC TGG CTC AG-3′) and reverse (1492R, GGT TAC CTT GTT ACG ACT-3′) primer (10mM each), 0.25μL of *Taq* polymerase (Takara), 36.75μL nuclease-free water, and 2μL of DNA template. The PCR conditions were: 94°C for 5 min followed by 30 cycles of amplification consisting of denaturation at 94°C for 30 sec, annealing at 58°C for 1 min, and extension at 72°C for 1.5 min.

PCR primers used were specific for the 515-806 bp region of the 16S rRNA encoding gene (**Table 5**) and contained Illumina 3′ adapter sequences as well as a 12-bp barcode. This barcode-based primer approach allowed sequencing of multiple samples in a single sequencing run without the need for physical partitioning. Sequencing was performed using an Illumina MiSeq DNA sequencer at Argonne National Laboratory's Next Generation Sequencing Core. Sequences were then trimmed and classified with the QIIME toolkit (version 1.8.0). Using the QIIME wrappers, OTUs were picked at 97% sequence identity using uclust and a representative sequence (centroid) was then chosen for each OTU by selecting the most abundant sequence in that OTU. These representative sequences were aligned using PyNAST and taxonomy was assigned to them using the uclust consensus taxonomy assigner. The PyNAST-aligned sequences were also used to build a phylogenetic tree with FastTree and weighted UniFrac distances then computed between all samples for additional ecological analyses, including principal coordinates analysis (PCoA).

Microarrays data and pathway analysis

Total RNA was reverse transcribed for cDNA synthesis, labeled and hybridized to Illumina (San Diego, CA, USA) MouseRef-8 v2 .0. Expression BeadChips with 25k probes and scanned using Illumina HiScan in the Functional Genomics Core of University of Chicago. Summary data were obtained using the BeadStudio software from Illumina. We evaluated the array quality and processed the data using the R/Bioconductor package "limma" for background correction and quantile normalization (19, 25). RNA samples used in this study passed the established quality criteria including an RNA Integrity Number greater than 7.5, and a 260nm/280nm optical density ratio above 1.8. We identified differentially expressed genes using

empirical Bayes statistics implemented by eBayes in "limma" package (20). The criteria of significance is set at False Discovery Rate (FDR) <5% and fold change >2.0. Microarray raw data and normalized data have been deposited in Gene Expression Omnibus database (http://www.ncbi.nlm.nih.gov/geo/) under accession number **GSE71997**.

Significant canonical pathways were identified using Ingenuity Pathway Analysis (IPA) software (Ingenuity Systems, Redwood City, CA). The significance of a canonical pathway was determined by the right-tailed (referring to the overrepresented pathway) Fisher's Exact Test with $p < 0.05$.

Histology / Histopathology Score / PAS / Ki-67 Immunofluorescence

Mucosal tissues were fixed in 4% formalin/PBS overnight. Five-micron sections were cut, deparaffinized in xylene, rehydrated, and stained with either H&E or Periodic Acid Schiff (PAS) base (Cat# 3952016 Sigma, St Louis, MO) and imaged on a Leica DM2500 microscope (Leica Microsystems, Wetzlar, Germany) through a 10X lens objective using Image Pro-Plus software (Media Cybernetics, Silver Springs, MD, USA) for image capture. Mucosal inflammation was blindly assessed by using the colitis scoring method previously described (2) and displayed as the disease activity score. To assess cell proliferation, Ki-67 staining was performed. Briefly, following rehydration, slides were heated in sodium citrate buffer (pH 6.0), blocked with blocking solution (Cat# x0909, Dako, Carpinteria, CA), and stained over night with Rabbit anti-Ki67 primary antibody (Cat# RM-9106, Thermo Scientific, Waltham, MA) in antibody dilluent (Cat# S3022, Dako). Slides were washed and incubated with donkey anti-rabbit secondary antibody (Cat# A31572, Alexafluor Life technologies) before counterstained and cover slipped with ProLong Gold anti-fade with DAPI (P36931, Thermo). Slides were processed and imaged in parallel and signal was semi-quantified blindly using ImageJ. Ki-67 signal was measured in 20-25 crypts per animal and displayed as mean fluorescent intensity/crypt.

Western Blot

Immunoblotting was performed as previously described (22) using the following antibodies: anti-TLR4 (sc-293072), anti-TLR2 (sc-10739), from Santa Cruz Biotechnology Inc. (Santa Cruz, CA); and anti-TNF-α (#3707) from Cell Signaling Technology Inc. (Boston, MA). All numerical results are expressed as the mean ± SEM of the indicated number of experiments. The results of blots are presented as direct comparisons of bands in autoradiographs and quantified by densitometry using ImageJ.

Enzyme-Linked Immunosorbent Assay

ELISA for TNFα protein on tissue homogenate was performed per manufacturer instructions (Cat 88-7324-22, eBiosciences, San Diego, CA).

Statistics

Data from the *in vivo* studies are presented as mean ± SEM; statistical significance was analyzed by the Analysis of Variance test (ANOVA) followed by analysis of significance (Tukey-Frame's multiple comparisons test) or T-test, where appropriate. $P<0.05$ was considered statistically significant, unless otherwise stated. 16S and microarray statistical analysis were performed as described above.

Results:

Self-Filling blind intestinal loops harbor a colon-like microbiome.

Ileal self-filling (SFL) or self-emptying (SEL) blind loops were surgically created in 8 week old WT, IL-$10^{-/-}$, TLR$4^{-/-}$, and IL-$10^{-/-}$/TLR$4^{-/-}$ C57Bl/6 mice and allowed to recover for 5 weeks. Gross inspection of SFL WT loops revealed distension with fecal contents and thickening of the bowel wall compared to the normal ileal appearance of SEL (**Fig 1a**). By 16S rRNA gene sequencing analysis, the SFL and SEL microbiota were significantly different ($P<0.0001$ using either ANOSIM or PERMANOVA), the former clustering in a manner similar to colonic microbiota of sham-operated colon, and the latter with sham-operated ileal microbiota, as shown by principal coordinate analysis (PCoA) of weighted UniFrac distances (**Fig 1b**). The SFL microbiota showed strong representation of *Bacteroidetes* and *Firmicutes,* whereas the SEL microbiota was more similar to that of sham-operated ileum (phylum level assignments in **Fig 1d**; family level in **Fig 9***)*.

To determine how the selected microbial communities would be impacted in a model of IBD using a genetically susceptible host, surgery was performed to create SEL and SFL in IL-$10^{-/-}$ mice, where approximately 15-20% develop spontaneous colitis after 12 weeks of age (9). Importantly, all IL-$10^{-/-}$ mice used for these experiments had normal ileal mucosa by gross visualization at the time of surgery. PCoA analysis again showed that the microbial community patterns in IL-$10^{-/-}$ SFL and SEL were highly comparable to the SFL and SEL observed in WT loops (**Fig 1c**) and SF clustered significantly different from SE ($P<0.0001$ using ANOSIM or PERMANOVA). This can also be shown by differences in taxonomic composition as well as in

measures of alpha diversity, specifically the Shannon diversity index (**Fig 1d & Fig 1e**). The diversity of microbiota in sham-operated colon, wild type SFL, and IL10$^{-/-}$ SFL microbiota was significantly higher than that in SEL and sham-operated ileum. These changes demonstrate that regardless of genetic background, SFL stasis, defined as accumulation of fecal contents, is a major driver of microbial structure; equally important, this microbiome is similar to that found in colon.

Changes in mucosal histology of self-filling loops resemble colonic mucosal structure.

Histological examination of SFL mucosa suggested differences with SEL and sham-operated ileum, characterized by elongation of crypt lengths, relative villus shortening, and increased goblet cell numbers that collectively provide resemblance of colonic mucosa (lower panels **Fig 1g & Fig 1h**). These changes were not always present and are also variably observed in the mucosa of the ileal pouch of UC patients who have undergone IPAA (12). In contrast, the SEL epithelium remained comparable to the sham ileal epithelium (upper panels, **Fig 1g & Fig 1h**).

Changes in mucosal gene expression in the self-filling ileal loop are consistent with colonic metaplasia.

To characterize molecular differences in mucosal tissues between SFL and SEL, illumina microarray analysis was performed. WT SFL exhibited suppression of immune response pathways, including regulation of antigen processing and presentation, cell surface receptor linked signal transduction, and proteolysis (**Table 1***)*. Despite these observed pathway differences, specific gene changes that would provide insights into the morphometric alterations in crypt depth and villous atrophy were not obvious (**Table 2***: Metaplasia-associated transcription changes in self-filling loops*). Therefore, we performed targeted analysis for morphogen-related genes that control intestinal architecture. Since Wnt-5a is required for crypt regeneration following mucosal injury and negatively regulates Sonic hedgehog (SHH), which is required for villous outgrowth, we hypothesized that non-canonical Wnt ligands were involved in our observed phenotype (11, 15). Indeed, Wnt5a gene expression was up-regulated while SHH was down-regulated in SFL compared with SEL (**Fig 1j**). Wnt-5a protein levels were altered in a consistent manner between SFL and SEL (**Fig 1k**). Expression of the gene for PDGFRα, a receptor responsible for epithelial proliferation, was significantly elevated in SFL. Consistently, the SFL demonstrated evidence of elevated cell proliferation compared with SEL, assessed by Ki-67 immunofluorescence (**Fig 1i**). Finally, analysis of the gene array results revealed unique

gene signatures for SFL and SEL, with global similarities observed between SFL and colonic transcriptomes as well as those observed between SEL and ileal transcriptomes (**Fig 1f**). Interestingly, these morphogen-related genes are also consistently altered in clinical human pouch biopsies compared with pre-pouch ileum as determined by RNAseq (unpublished data). This study supports the notion that, in the presence of stasis-induced colonic-like microbiota, the SFL develops both colon-like histologic features and certain colon-like gene expression changes (differentially expressed genes and pathway analysis from WT SFL and SEL are shown in **Table 2**).

Active mucosal inflammation and metaplasia occur in the self-filling loop, but not in the self-emptying loop, of the IL-10$^{-/-}$ mouse.

To examine the impact of stasis-induced colon-like microbiota on a background of genetic susceptibility, we examined the colonic mucosa and inflammatory state of the SFL and SEL in the IL-10$^{-/-}$ mouse. In a manner similar to WT, IL-10$^{-/-}$ SFL adopt a colon-like mucosal architecture compared with SEL (**Fig 2a**) and showed similar changes in Wnt-5a, SHH, and PDGFRα morphogen-related gene expression (**Fig 2f**). IL-10$^{-/-}$ SFL also displayed elevated proliferation compared with SEL, assessed by Ki-67 (**Fig 2c & Fig 2d**). However, there were at least three distinct differences between WT and IL-10$^{-/-}$ mice. First, while WT mice do not develop active mucosal inflammation, IL10 $^{-/-}$ SFL exhibit evidence of lymphoplasmacytic infiltrates and histological inflammation (**Fig 2a & Fig 2e**). Second, IL-10$^{-/-}$ SFL showed a loss of goblet cells compared with SEL or WT SFLs (**Fig 2b**), consistent with an inflamed mucosa phenotype. Finally, the IL-10$^{-/-}$ mice with SFL exhibited severe weight loss, cachexia, and anorexia. In contrast, the SEL mucosa of IL-10$^{-/-}$ mice remained similar to sham ileum and demonstrated little histologically observable inflammation.

Dramatic changes in key pro-inflammatory cytokines accompanied the histological inflammation and clinical deterioration in IL-10$^{-/-}$ SFL. Thus transcript levels for IFNγ, TNFα, and IL-1β (**Fig 2g**) were significantly elevated compared with SEL and WT animals. In contrast to IL-10$^{-/-}$ SEL or WT SFL, pathway analysis of gene microarray data in IL-10$^{-/-}$ SFL showed increases in antigen processing, host defense, and immune response genes (**Table 3**). Individual genes exhibiting significant differences (defined as >2.0 fold change) between IL-10$^{-/-}$ SFL and SEL are displayed in **Table 4**.

To verify our histological findings in a second relevant model of colonic inflammation, we used the well-characterized model of DSS administration to non-genetically susceptible WT

mice, where inflammation is normally only observed in the colon after providing 2% DSS in drinking water for 3 days. Interestingly, DSS causes inflammation of the WT SFL, but not the SEL, providing additional parallels between the SFL and colon (**Fig 3**).

Together, these data strongly indicate that the stasis-induced changes in gut microbiota, while sufficient for inducing intestinal metaplasia, were insufficient alone to cause inflammatory disease, suggesting that a 'second hit' provided by genetically (IL-10$^{-/-}$) or environmentally-induced (DSS) changes are required to induce inflammation.

Innate immunity pathways involving TLR-4 mediate intestinal metaplasia and mucosal inflammation in self-filling loops.

Since the SFL displays epithelial metaplasia and altered inflammatory pathways in the presence of greater bacterial loads and diversity as compared to SEL, we assessed mucosal toll-like receptors, which are responsible for microbial recognition and downstream inflammation. TLR4 mRNA transcript and protein expression were significantly elevated in SFL of both genotypes, yet were higher in IL-10$^{-/-}$ than WT (**Fig 2i**). There were no significant differences in TLR2 in WT SEL or SFL, however TLR2 was also significantly elevated in SFL compared with SEL in IL-10$^{-/-}$ mice. Consistent with these observations, gene microarray demonstrated elevated expression of pro-inflammatory gene pathways in IL-10$^{-/-}$ SFL compared with IL-10$^{-/-}$ SEL (**Fig 2h**). These observations are consistent with the pathway analysis and differentially expressed inflammatory genes shown in **Tables 3&4**, where numerous immune pathways are over-expressed in IL-10$^{-/-}$ SFL.

Given the colon-like epithelium associated with up-regulated TLR4 in SFL, we examined the role of TLR4 in mediating the observed changes in the SFL using TLR4$^{-/-}$ mice. Surprisingly, the histological features of SFL and SEL of TLR4$^{-/-}$ mice were not obviously different from that of sham-operated ileum (**Fig 4a vs. Fig 1g**). Along with the lack of metaplastic changes in TLR4$^{-/-}$ SFL mice, no significant differences were observed in SHH and Wnt5a gene expression as compared to WT SFL mice (**Fig 4b**) Similarly, no differences in IFNγ or TNFα expression were found (**Fig 4c**) as compared to IL10$^{-/-}$ SFL. In contrast to WT and IL-10$^{-/-}$ animals, there were no differences in crypt Ki-67 signal between SFL and SEL in TLR4$^{-/-}$ animals (data not shown). The SFL of one of 3 TLR4$^{-/-}$ animals showed variability in the metaplasia gene signature and the colon gene signature, with profiles more akin to WT SFL and sham colon rather than ileum (**Fig 6a & 6b**). In contrast to the lack of host adaptation, it is important to note that the relative microbiota profiles of TLR4$^{-/-}$ mice were significantly different between SFL and SEL ($P<0.014$

and P<0.007 using ANOSIM and PERMANOVA, respectively), similar to the microbiota profiles of WT and IL-10-/- mice (phylum level shown in **Fig 4d**; family level shown in **Fig 10**; *WT phylum level shown in **Fig 1d***). Collectively, these results suggest TLR4 signaling plays an important role in mediating the metaplastic changes that occur in response to stasis and that stasis remains the dominant driver of microbial community structure over the TLR4$^{-/-}$ host genotype.

To further examine the TLR4 dependence of the colonic-like metaplasia and inflammation in mice genetically prone to inflammation, SFL and SEL were studied in IL-10$^{-/-}$/TLR4$^{-/-}$ double KO mice. Similar to the TLR4$^{-/-}$ mice, SF loops in IL-10$^{-/-}$/TLR4$^{-/-}$ showed no signs of metaplasia (**Fig 4e**), no changes in expression of the morphology-related genes Wnt-5a, SHH, and PDGFRα (**Fig 4f**), and no changes in inflammatory genes, IFNγ and TNFα (**Fig 4g**) compared with SEL mucosa. This strongly indicates that the observed changes in the IL-10$^{-/-}$ SFL rely heavily upon TLR4 signaling.

Microbes from self-filling loops cause heightened colonic morphology in germ-free WT mice and colitis in germ-free IL-10 deficient mice

To determine the differential effects of SFL and SEL microbiota on the colonic epithelia, we examined morphological and inflammatory outcomes of colonic tissue in conventionalized germ-free (GF) mice. It is well documented that in GF animals, colonic epithelial development is incomplete, with shortened crypt depth, atrophied villi, and fewer goblet cells. We conventionalized WT GF mice with SFL or SEL contents (Fig 5a). After 4 weeks, GF mice conventionalized with SFL contents induced hypertrophy of the muscle layer, increased neuronal fibers, and altered gastrointestinal motility compared with GF mice conventionalized with SEL luminal contents (unpublished Chang lab data). In addition, morphogen-related gene expression (Wnt5a, SHH) was altered in a pattern similar to that observed in SFL and SEL mucosae (**Fig 7**), with greater Wnt-5a and decreased SHH following colonization with SFL microbiota.

As described, microbial stasis induced severe inflammation in the IL-10$^{-/-}$ SFL and led to a mucosa with some degree of colon-like resemblance. To test if SFL microbes alone drive the IL-10$^{-/-}$ inflammatory response, we conventionalized germ-free IL-10$^{-/-}$ and WT mice with microbes from WT SFL and SEL. Following conventionalization, IL-10$^{-/-}$ colons displayed greater mucosal thickness than WT mice making the colonic cross section larger. Conventionalization of germ-free IL-10$^{-/-}$ mice with SFL microbes induced severe active colitis, characterized by

increased lymphoplasmacytic infiltrates and crypt abscesses. In contrast, SEL microbes failed to induce disease (**Fig 5a and 5b**); in contrast, CONV of WT mice with SFL contents resulted in no active colonic inflammation as determined by blinded histology inflammation score assessment (**Fig 5b**). Consistent with histology, colonic epithelial expression of pro-inflammatory markers, including IFNγ, TNFα, and TLR4 gene expression were significantly greater in IL-10$^{-/-}$ germ-free mice conventionalized with SFL microbes compared with all other groups (**Fig 5c**).

These results support the observation that select and specific microbial community composition modifies colonic morphology in germ free animals and causes aberrant mucosal inflammatory response in genetically-susceptible hosts.

Human correlations to morphogenic and microbial data is consistent with results from the mouse model

To correlate our findings in the mouse model of pouchitis with human samples, we obtained pouch biopsies and fecal samples from patients with previous total abdominal colectomies and IPAA. We first compared human microbiota samples to murine loops using 16S rRNA gene analysis. While microbial genera from ileum, cecum, and distal colon in sham mice remain somewhat distinct from human pouch samples, microbial communities from WT and IL-10$^{-/-}$ SF loops appear compositionally most similar to human pouch samples (phylum level assignments shown in **Fig 5d**; family level shown in **Fig 9**). PCoA analysis further demonstrated microbial community clustering between SFL samples and human samples (**Fig 8**), while the other samples cluster more similarly. Because we did not have human pre-pouch 16S rRNA gene samples that could be included in this analysis, our interpretation is limited the conclusion that the human pouch samples are more similar to murine SFL than they are to murine SEL communities. Finally, human ileal pouches exhibit morphology-related gene responses that are similar to those observed in the murine SFL, with elevated Wnt-5a and PDGFRα expression, as compared to normal human pre-pouch ileum (**Fig 5e**).

Discussion:

Ulcerative colitis (UC) never involves the small intestine and total colectomy is curative. However, as nature would have it, at least half of patients who undergo ileal pouch anal anastomosis ((PAA), a procedure that involves the creation of a pseudorectum from the terminal ileum, will develop within 1-2 years an inflammatory condition called UC (1, 6). Many believe that the development of condition is a recapitulation of some of the same pathophysiological

processes that caused the original UC because it has many of the endoscopic and histologic features of the original disease and it occurs much less commonly in non-IBD (Familial Adenomatous Polyposis, FAP) patients who undergo the same procedure. Even in these patients, the FAP pouchitis looks different and often has a milder clinical course compared to UC pouchitis. However, if UC only involves colonic tissue, why would UC pouchitis develop in the ileal mucosa of the pouch? This question remains unanswered although the notion that the pouch mucosa undergoes a colonic-type metaplasia has often been theorized. This study now provides molecular evidence to support this hypothesis. Using a murine model that reproduces many of the same conditions in UC, we show that the co-occurrence of a colonic epithelial transcriptome, the assemblage of a colonic-like microbiome, and genetic susceptibility are all key factors that can result in the development of a UC-like inflammatory response. Each process by itself, however, is insufficient in causing disease.

The development of a colonic-like microbiome characterized by greater bacterial load and increased membership by *Bacteroidetes* and *Firmicutes* (**Fig.1d**) is almost certainly a consequence of intestinal stasis, a condition shared between normal murine colon and murine SF blind loop, and is similar to the microbiome profile of healthy humans (23). The similar composition between our murine SF loop microbial community and human pouch samples, compared with SE loop samples, further supports that this is a general phenomenon of stasis rather than being species- or disease-specific. The fact that the SE blind loop, which is identical in everyway with the SF loop except for the propagative direction of intestinal content, does not develop a colonic-like microbiota strongly supports this notion. In addition, antibiotic treatment prevents the development of colonic-like metaplasia in the SF loop (data unpublished).

In response to the colonic-like microbiota, the general SFL mucosal morphology and gene expression diverge away from normal small intestine and towards a colonic-like phenotype (**Fig.1g**). This observation is consistent with a previous report suggesting the presence of fecal anaerobic bacteria is associated with colonic-like morphology in human pouches (10). The changes in gene expression of key morphogens such as Wnt5a and SHH in SFL provide molecular explanation for the development of the observed colon-like metaplasia. Together these data illustrate the highly adaptable nature of the intestinal mucosa to alter with shifting microbial communities.

In health, small intestinal epithelial cells and lamina propria lymphoid cells maintain low

expression of TLR4 and TLR2 to prevent over-responsive immune activation. However, elevated TLR4 and TLR2 levels have been reported in active human pouchitis samples (17, 21). While TLR4 expression was elevated in WT SFL, it was not associated with alterations in molecular or histological markers of inflammation. On the contrary, WT SF loops display down-regulated gene expression of immune signaling pathways, most notably those suppressing antigen processing and presentation. Since *Bacteroides* are elevated in the SF loop microbiota, and these commensal genera are known stimulators of IL-10 producing CD-4 T cells (13), we posit that an IL-10-mediated mechanism for WT tolerance. Murine IL-10 is known to inhibit Th1 mediated pathways by supporting Th2 responses. Polymorphisms of the IL-10 and IL-1p receptor have been associated with increased risk for IBD and very early onset ulcerative colitis. In IL-$10^{-/-}$ mice, we typically observe an incidence of 15-20% for the development of spontaneous chronic colitis, although this rate can be highly influenced by environmental, dietary and microbial factors. For these experiments, it is a useful model of genetic susceptibility which is also considered to be a conditional requirement for the development of IBD (9).

Our data demonstrate that in marked contrast to WT SF loops, the SF loops of IL-$10^{-/-}$ deficient mice manifest elevated signaling of numerous innate and adaptive immune pathways, including bacterial sensing and processing pathways, and elevated pro-inflammatory cytokines. On a background of IL-$10^{-/-}$ deficiency, severe histological injury in the SFL mucosa develops whereas the SEL tissue remains largely non-inflamed (**Fig 2 & Tables 3&4**). However, there are a number of limitations to our interpretation. First, the current study examined loops at 5 weeks post-surgical placement and it is possible that WT mice would eventually develop inflammatory responses, which are more immediately robust under IL-$10^{-/-}$ susceptibility. We have, however, collected WT SFL tissues at 50 days post-surgery and find little evidence of infiltrates or epithelial erosion at that time point (unpublished). IL-$10^{-/-}$ animals, on the other hand, cannot tolerate SFL beyond 35 days, so the 5-week endpoint was chosen in this report. Another potential confounder is that the increased relative abundance of the *Proteobacteria* family *Enterobacteriaceae* observed in IL-$10^{-/-}$ SFL compared with WT SFL mice could play a role in the disease pathogenesis (4), although this family is still observed in IL-10-/- SEL that do not have severe disease.

Since inducible TLR4 levels were observed in SF loops of both WT and IL-$10^{-/-}$ mice, we tested the role of TLR4 signaling in mucosal hyperplastic remodeling and inflammation using TLR4-deficient mice. The absence of morphological remodeling at the histological and transcriptional level suggests mucosal sensing of microbes through this TLR pathway drives the metaplasia transcriptional responses changes in the SF ileum (**Fig 4 a,b, & Fig.6**). Interestingly,

IL-10$^{-/-}$/TLR4$^{-/-}$ mice failed to exhibit both metaplasia and inflammatory disease in SF loops compared with SE loops (**Fig 4f&g**). We had anticipated the possibility of inflammation since others previously described spontaneous colitis associated with adenoma-carcinoma formation in IL-10$^{-/-}$/TLR4$^{-/-}$ mouse colons as early as 3-6 months of age (7, 26). However, in our work, no colonic inflammation (thickening, opaqueness) or adenomas were visible at the time of harvest (3 months). In the ileum of IL-10$^{-/-}$/TLR4$^{-/-}$ mice, the lack of inflammation or adaptation in SF loops suggests TLR4 has fundamentally important regulatory roles in driving ileal inflammation (and colonic-like metaplasia) following stasis.

The microbial communities of the SF loops are also functionally different in that they proved to be colitogenic in IL10$^{-/-}$ germ free mice. Further examination revealed that SFL contents induced hypertrophy of the muscle layer, increased neuronal fibers, and altered gastrointestinal motility compared with SE contents (unpublished Chang lab data). Additionally, the colonic mucosal expression of the morphology-related genes, Wnt-5a and SHH, were altered in a pattern similar to the murine SF vs. SE loop expression (**Fig 7**).

In conclusion, this mouse model recapitulates many of the features of the pouch in UC patients following total proctocolectomy with IPAA. An important correlate is that much like the mouse SFL, the IPAA pouch in UC sometimes acquires 'colon-like' characteristics, including the development of a colonic-like microbiota. This in turn, in part via a TLR4-dependent pathway, leads to alterations in mucosal morphology that resemble colon and, indeed, transcriptional analysis supports that notion that the SFL has functionally and immunologically adapted to become colon mucosa. In genetically susceptible hosts, here represented by IL10$^{-/-}$ deficient mice, the colonic microbial community triggers an inflammatory response in the 'colon-ized' SFL. Our studies suggest that these changes are related in that the development of a colon-like phenotype occurs in both humans and mice and is a result of the stasis-induced conditions that favor the assemblage of a colonic-like microbiota. These findings provide a new paradigm for our understanding of IBD-associated pouchitis and the mechanisms responsible for disease pathogenesis in a region of intestine never affected by UC prior to total colectomy and IPAA.

Author Contributions:

J.C.A, E.B.C, D.T.R, N.H and M.A.W designed research studies, M.A.W, J.F.P, R.F.L, B.D.S., S.R.D, and L.A.R conduced *in vivo* experiments and bench work, Y.H., C.R.W, V.A.L, M.W.M, G.C.A, M.L.S, and D.A.A. acquired data, Y.H, M.A.W, J.F.P, and D.A.A analyzed data, and E.B.C, J.F.P, M.C.R, and J.C.A. wrote the manuscript.

Funding acknowledgment: NIDDK DK42086 (DDRCC), UH3 DK083993, Leona and Harry Helmsley Trust (SHARE), R37 DK47722, T32 DK07074, F32 DK105728, Gastrointestinal Research Foundation of Chicago, Peter and Carol Goldman Family Research grant.

Figure and Table Legend

Figure 1 – Self-filling loops adopt a colon architecture, transcript, and microbiome.

(a) The gross appearance of the self-filling (SFL) and self-emptying (SEL) loops, where peristalsis (black arrow) drives towards or away from the blind end; (b) Principal coordinate analysis (PCoA) using weighted UniFrac of microbial communities from WT SFL and SEL demonstrates clustering with sham colon and ileum, respectively; (c) PCoA analysis of IL-10$^{-/-}$ SFL and SEL microbial community clustering with sham colon and ileum, respectively; (d) taxonomic analysis of microbial genera by group; (e) Shannon diversity index from microbial communities by group; (f) microarray gene signatures demonstrate global transcriptional similarity between SH-I and WT-SEL and between SH-C:WT-SFL, where red = up-regulated genes and blue = down-regulated genes; (g) representative histology sections from sham ileum (SH-I), WT-SEL loop (WT-E), sham colon (SH-C) and WT-SFL loop (WT-F), where SH-I and WT-SEL appear similar while SH-C and WT-SEL appear similar; (h) PAS stain of WT-SEL and WT-SFL; (i) Ki-67 immunoflourescence of WT-SEL and WT-SFL, with Ki67 (Red) and DAPI (Blue); (j) mRNA expression for the morphology genes, Wnt-5a, SHH, and PDGFRα, were significantly altered between SFL and SEL (n=3); (k) In addition to different Wnt-5a protein levels (representative Western blots). Data are expressed as the means ± SEM. *P<0.05 vs WT-SEL unless otherwise stated. Scale bar = 100 μm

Figure 2 – Il-10-/- self-filling loops are susceptible to mucosal inflammation.

(a) Representative histology sections of the IL-10$^{-/-}$ SEL (10KO-SEL) and SFL (10KO-SFL), where SFL demonstrate mucosal inflammation and inflammatory infiltrates; (b) PAS stain of 10KO-SFL and 10KO-SEL; (c) Ki-67 immunoflourescence of 10KO-SEL and 10KO-SFL, with Ki67 (Red) and DAPI (Blue); (d) quantified Ki-67 intensity per crypt; (e) blinded histology score of the SFL and SEL from WT and IL-10$^{-/-}$ mice; (f) expression of morphology genes, Wnt-5a, SHH, and PDGFRα, were significantly altered between IL-10$^{-/-}$ SFL and SEL; (g) cytokine expression of IL-1β, TNFα, and IFN-γ was significantly elevated in IL-10$^{-/-}$ SFL compared with all other groups; (h) numerous inflammatory-associated genes were differentially expressed in IL-10$^{-/-}$ SFL compared with WT SF loops, where red = up-regulated and blue= down-regulated; (i) expression and protein levels of TLR4 were significantly elevated in SFL compared to SEL in both genotypes, however, total levels were significantly greater in IL-10$^{-/-}$. TLR2 expression and protein levels were significantly elevated in IL-10$^{-/-}$ SFL loops compared with SEL, but no

changes were observed in WT. Data are expressed as the means ± SEM. *P<0.05 vs 10KO-SEL unless otherwise stated. Scale bar = 100 μm

Figure 3 – DSS indues inflammation in Wild-type self-filling loops.

Compared with control WT SFL, the administration of 2% DSS in drinking water for 3 days significantly induced mucosal injury and TNFα protein levels in WT SFL, but not WT SEL despite slightly elevated TNFα. Colonic injury was also visible and colonic TNFα protein levels were significantly elevated in all animals administered DSS. *P < 0.05. Scale bar = 100 μm.

Figure 4 – Self-filling loop morphology and inflammation requires TLR4 signaling.

(a) Representative histology of TLR4$^{-/-}$ SFL (T4KO-F) and SEL (T4KO-E) demonstrated normal mucosal architecture; (b) compared with WT SEL, TLR4$^{-/-}$ demonstrate no differences in morphology genes, SHH and Wnt-5a; (c) compared with IL-10$^{-/-}$ SFL, TLR4$^{-/-}$ demonstrate no differences in pro-inflammatory genes, TNFα and IFN-γ; (d) the composition of loop microbial genera in TLR4$^{-/-}$ mice remained similar to WT mice and cluster with SFL and SEL samples respectively; (e) Representative histology of TLR4/IL-10$^{-/-}$ SFL and SEL also demonstrated normal mucosal architecture; (f) no differences were observed in morphology gene expression between TLR4/IL-10$^{-/-}$ SFL and SEL; (g) no differences were observed in pro-inflammatory cytokine expression between TLR4/IL-10$^{-/-}$ SFL and SEL. Data are expressed as the means ± SEM. *P < 0.05 vs T4KO-SFL. Scale bar = 100 μm.

Figure 5 – Self-filling loop microbes induce colitis in IL-10-/- germ-free mice and self-filling loops resemble human samples.

(a) Representative histology of colons from WT germ free (GF) and IL-10$^{-/-}$ germ free (GF 10KO) mice conventionalized with contents from SFL or SEL. GF 10KO colons exhibited inflammation with abscess (inset), crypt dysplasia (dotted arrow), and luminal neutrophils and mucosal lymphoplasmacytic cells (dashed arrow); (b) blinded histology of colon mucosa from conventionalized WT or IL-10 mice; (c) IFN-γ, TNFα, and TLR4 expression was significantly higher in GF IL-10$^{-/-}$ mice conventionalized with SF contents compared with all other groups; (d) Microbial community composition of samples from murine and human samples, where human pouch samples were similar to murine Sham Colon (SH-C) and WT and IL-10 KO SFL contents compared with sham ileum (SH-I) or WT and IL-10 KO SEL contents; (e) compared with human pre-pouch ileal biopsies, human pouch biopsies differentially expressed the morphology genes

Wnt-5a and PDGFRα similar to the pattern observed in murine SFL vs SEL loop mucosa. Data are expressed as the means ± SEM. Scale bar = 100 μm.

Figure 6 – Self-filling loop gene signatures are abated without TLR4.

Metaplasia and colonic gene signatures. Microarray gene targets (25k probes) were quantified and normaliz to the average signal within each sample. Altered genes are displayed as red = up-regulation; blue = down-regulation. Criteria of significance is set at False Discovery Rate (FDR) <5% and fold change (FC_{log2}) >2.0. Analysis of differentially expressed microarray genes demonstrated a blunted response in the $TLR4^{-/-}$ SFL loops compared with the more robust change in WT SFL samples (a). Similarly, colon-associated gene signatures that are evident in the WT SFL loops (**Fig 1f** and **Table 3**) are less robust in $TLR4^{-/-}$ SFL loop samples (b).

Figure 7 – Morphology-related genes in conventionalized germ-free colons.

Conventionalization of germ free mice with SFL or SEL loop contents significantly altered the morphology genes Wnt-5a and SHH in a similar pattern to what is observed in SFL and SEL loop tissues, respectively. Conventionalization of germ-free WT animals with microbes from SFL resulted in greater Wnt-5a and lower SHH compared with conventionalization with microbes from SEL. n=4/group. *P<0.05.

Figure 8 – Human and mouse microbial principal coordinate analysis.

Principal coordinate analysis (PCoA) based on weighted UniFrac of murine and human microbiota samples. Compared with human pouch samples (n=22), murine WT SFL (n=18) and IL-10-/- SFL (n=3) samples globally cluster most closely while WT SEL (n=18) and IL-10 SEL (n=3) samples and all sham samples (ileum, n=5; cecum, n=5; and distal colon, n=5) cluster more similarly.

Figure 9 – 16S family taxonomic analysis for data shown in Fig 1d.

Color coding of relative microbial abundances at the family level is displayed for each sample type. Generally, the SFL and colon samples (WT-SH-C) display greater levels of *Bacteroidetes* families compared with the *Firmicutes* and *Proteobacteria* families, which are more dominant in SEL and Ileum samples (WT-SH-I). Similarily, while different bacterial families dominant the human vs mouse samples, the Pouch has a similar Phylum composition to SFL.

Figure 10 – 16S family taxonomic analysis for data shown in Fig 4d.

Color coding of relative microbial abundances at the family level is displayed for each sample type. In contrast to little histological changes, compared with the T4KO-SEL the T4KO-SFL displayed an increased relative abundance of *Bacteriodetes* and fewer *Firmicutes*, suggesting the microbial populations are shifting in composition in response to the stasis environment, regardless of host mucosal phenotype.

Table 1 - Self-filling loop tissues mimic colon transcript patterns.

Pathways analysis of microarray results from loop tissues demonstrated WT SFL mucosa express colon-associated gene patterns compared with WT SEL loops (Top). Specifically these altered genes suggested decreases in pathways associated with immune activation (Bottom). Differentially expressed genes are displayed where red = up-regulated genes; blue = down-regulated genes. Microarray targets (25k probes) were quantified and normalized to the average signal within each sample. The criteria of significance is set at False Discovery Rate (FDR) <5% and fold change (FC_{log2}) >2.0.

Table 2 – Metaplasia-associated transcription changes in self-filling loops.

Significantly altered metaplasia-associated genes in WT SFL loops compared with WT SEL loops. WT SFL loops induced differential gene patterns compared with WT SEL loops that included significantly up and down regulated genes (A). Specific genes differentially expressed in WT-SFL loops compared with WT-SEL loops (B). Red = up-regulated genes; blue = down-regulated genes. Microarray targets (25k probes) were quantified and normalized to the average signal within each sample. The criteria of significance is set at False Discovery Rate (FDR) <5% and fold change (FC_{log2}) >2.0.

Table 3 - IL-10$^{-/-}$ SFL vs. SEL and IL-10$^{-/-}$ vs. WT gene pathway changes.

Pathway analysis of microarray results from IL-10$^{-/-}$ loop tissue demonstrated up-regulation of immune associated pathways in SFL compared with SEL tissue (Top). Similarly, compared with WT SFL, Il-10$^{-/-}$ SFL demonstrated up-regulation of numerous immune pathways and attenuation of others (Bottom). Red = up-regulated genes; blue = down-regulated genes. Microarray targets (25k probes) were quantified and normalized to the average signal within each sample. The criteria of significance is set at False Discovery Rate (FDR) <5% and fold change (FC_{log2}) >1.5.

Table 4 – List of differentially expressed genes in IL-10$^{-/-}$ SFL vs SEL.

List of differentially expressed inflammatory genes from microarray analysis are displayed for IL-$10^{-/-}$ SFL compared to Il-$10^{-/-}$ SEL tissues. Red = up-regulated genes; blue = down-regulated genes. Microarray targets (25k probes) were quantified and normalized to the average signal within each sample. The criteria of significance is set at False Discovery Rate (FDR) <5% and fold change (FC_{log2}) >2.0.

Table 5 – Primers used in this study.

Bibliography

1. **Angriman I**. Relationship between pouch microbiota and pouchitis following restorative proctocolectomy for ulcerative colitis. *World J Gastroenterol* 20: 9665, 2014.

2. **Bennebroek Evertsz' F, Nieuwkerk PT, Stokkers PCF, Ponsioen CY, Bockting CLH, Sanderman R, Sprangers MAG**. The patient simple clinical colitis activity index (P-SCCAI) can detect ulcerative colitis (UC) disease activity in remission: a comparison of the P-SCCAI with clinician-based SCCAI and biological markers. *J Crohns Colitis* 7: 890–900, 2013.

3. **Devkota S, Wang Y, Musch MW, Leone V, Fehlner-Peach H, Nadimpalli A, Antonopoulos DA, Jabri B, Chang EB**. Dietary-fat-induced taurocholic acid promotes pathobiont expansion and colitis in Il10-/- mice. *Nature* 487: 104–8, 2012.

4. **Garrett WS, Gallini CA, Yatsunenko T, Michaud M, DuBois A, Delaney ML, Punit S, Karlsson M, Bry L, Glickman JN, Gordon JI, Onderdonk AB, Glimcher LH**. Enterobacteriaceae act in concert with the gut microbiota to induce spontaneous and maternally transmitted colitis. *Cell Host Microbe* 8: 292–300, 2010.

5. **Gionchetti P, Calafiore A, Riso D, Liguori G, Calabrese C, Vitali G, Laureti S, Poggioli G, Campieri M, Rizzello F**. The role of antibiotics and probiotics in pouchitis. [Online]. *Ann Gastroenterol Q Publ Hell Soc Gastroenterol* 25: 100–105, 2012. http://www.pubmedcentral.nih.gov/articlerender.fcgi?artid=3959382&tool=pmcentrez&rendertype=abstract [5 Oct. 2015].

6. **Gionchetti P, Rizzello F, Helwig U, Venturi A, Lammers KM, Brigidi P, Vitali B, Poggioli G, Miglioli M, Campieri M**. Prophylaxis of pouchitis onset with probiotic therapy: a double-blind, placebo-controlled trial. [Online]. *Gastroenterology* 124: 1202–9, 2003. http://www.ncbi.nlm.nih.gov/pubmed/12730861 [5 Oct. 2015].

7. **González-Navajas JM, Fine S, Law J, Datta SK, Nguyen KP, Yu M, Corr M, Katakura K, Eckman L, Lee J, Raz E**. TLR4 signaling in effector CD4+ T cells regulates TCR activation and experimental colitis in mice. *J Clin Invest* 120: 570–81, 2010.

8. **Jostins L, Ripke S, Weersma RK, Duerr RH, McGovern DP, Hui KY, Lee JC, Schumm LP, Sharma Y, Anderson CA, Essers J, Mitrovic M, Ning K, Cleynen I, Theatre E, Spain SL, Raychaudhuri S, Goyette P, Wei Z, Abraham C, Achkar J-P, Ahmad T, Amininejad L, Ananthakrishnan AN, Andersen V, Andrews JM, Baidoo L, Balschun T, Bampton PA, Bitton A, Boucher G, Brand S, Büning C, Cohain A, Cichon S, D'Amato M, De Jong D, Devaney KL, Dubinsky M, Edwards C, Ellinghaus D, Ferguson LR, Franchimont D, Fransen K, Gearry R, Georges M, Gieger C, Glas J, Haritunians T, Hart A, Hawkey C, Hedl M, Hu X, Karlsen TH, Kupcinskas L, Kugathasan S, Latiano A, Laukens D, Lawrance IC, Lees CW, Louis E, Mahy G, Mansfield J, Morgan AR, Mowat C, Newman W, Palmieri O, Ponsioen CY, Potocnik U, Prescott NJ, Regueiro M, Rotter JI, Russell RK, Sanderson JD, Sans M, Satsangi J, Schreiber S, Simms LA, Sventoraityte J, Targan SR, Taylor KD, Tremelling M, Verspaget HW, De Vos M, Wijmenga C, Wilson DC, Winkelmann J, Xavier RJ, Zeissig S, Zhang B, Zhang CK, Zhao H, Silverberg MS, Annese V, Hakonarson H, Brant SR, Radford-Smith G, Mathew CG, Rioux JD, Schadt EE, Daly MJ, Franke A, Parkes M, Vermeire S, Barrett JC, Cho JH**. Host-microbe interactions have shaped the genetic architecture of inflammatory bowel disease. *Nature* 491: 119–24, 2012.

9. **Kühn R, Löhler J, Rennick D, Rajewsky K, Müller W**. Interleukin-10-deficient mice develop chronic enterocolitis. [Online]. *Cell* 75: 263–74, 1993. http://www.ncbi.nlm.nih.gov/pubmed/8402911 [6 Jun. 2015].

10. **Kuisma J, Mentula S, Luukkonen P, Jarvinen H, Kahri A, Farkkila M**. Factors associated with ileal mucosal morphology and inflammation in patients with ileal pouch-anal anastomosis for ulcerative colitis. *Dis Colon Rectum* 46: 1476–83, 2003.

11. **Madison BB, Braunstein K, Kuizon E, Portman K, Qiao XT, Gumucio DL**. Epithelial hedgehog signals pattern the intestinal crypt-villus axis. *Development* 132: 279–89, 2005.

12. **Marmorale C, Guercioni G, Siquini W, Freddara U, Santinelli A, Rubini C, Carle F, Landi E**. Evolution of the changes of the ileal pouch mucosa over a long follow-up period. [Online]. *Hepatogastroenterology* 50: 1370–5 http://www.ncbi.nlm.nih.gov/pubmed/14571740 [4 Aug. 2015].

13. **Mazmanian SK, Round JL, Kasper DL**. A microbial symbiosis factor prevents intestinal inflammatory disease. *Nature* 453: 620–5, 2008.

14. **Mesbah-Uddin M, Elango R, Banaganapalli B, Shaik NA, Al-Abbasi FA**. In-Silico Analysis of Inflammatory Bowel Disease (IBD) GWAS Loci to Novel Connections. *PLoS One* 10: e0119420, 2015.

15. **Miyoshi H, Ajima R, Luo CT, Yamaguchi TP, Stappenbeck TS**. Wnt5a potentiates TGF-β signaling to promote colonic crypt regeneration after tissue injury. *Science* 338: 108–13, 2012.

16. **Ng SC, Bernstein CN, Vatn MH, Lakatos PL, Loftus E V, Tysk C, O'Morain C, Moum B, Colombel J-F**. Geographical variability and environmental risk factors in inflammatory bowel disease. *Gut* 62: 630–49, 2013.

17. **Scarpa M, Grillo A, Pozza A, Faggian D, Ruffolo C, Scarpa M, D'Incà R, Plebani M, Sturniolo GC, Castagliuolo I, Angriman I**. TLR2 and TLR4 up-regulation and colonization of the ileal mucosa by Clostridiaceae spp. in chronic/relapsing pouchitis. *J Surg Res* 169: e145–54, 2011.

18. **Scharl M, Rogler G**. Microbial sensing by the intestinal epithelium in the pathogenesis of inflammatory bowel disease. *Int J Inflam* 2010: 671258, 2010.

19. **Shi W, Oshlack A, Smyth GK**. Optimizing the noise versus bias trade-off for Illumina whole genome expression BeadChips. *Nucleic Acids Res* 38: e204, 2010.

20. **Smyth GK, Michaud J, Scott HS**. Use of within-array replicate spots for assessing differential expression in microarray experiments. *Bioinformatics* 21: 2067–75, 2005.

21. **Toiyama Y, Araki T, Yoshiyama S, Hiro J, Miki C, Kusunoki M**. The expression patterns of Toll-like receptors in the ileal pouch mucosa of postoperative ulcerative colitis patients. *Surg Today* 36: 287–90, 2006.

22. **Wang Y, Devkota S, Musch MW, Jabri B, Nagler C, Antonopoulos DA, Chervonsky A, Chang EB**. Regional mucosa-associated microbiota determine physiological expression of TLR2 and TLR4 in murine colon. *PLoS One* 5: e13607, 2010.

23. **Weir TL, Manter DK, Sheflin AM, Barnett BA, Heuberger AL, Ryan EP**. Stool microbiome and metabolome differences between colorectal cancer patients and healthy adults. *PLoS One* 8: e70803, 2013.

24. **Wells JM, Loonen LMP, Karczewski JM**. The role of innate signaling in the homeostasis of tolerance and immunity in the intestine. *Int J Med Microbiol* 300: 41–8, 2010.

25. **Xie Y, Wang X, Story M**. Statistical methods of background correction for Illumina BeadArray data. *Bioinformatics* 25: 751–7, 2009.

26. **Zhang R, Li Y, Beck PL, McCafferty D-M**. Toll-like receptor 4 regulates colitis-associated adenocarcinoma development in interleukin-10-deficient (IL-10(-/-)) mice. *Biochem Soc Trans* 35: 1375–6, 2007.

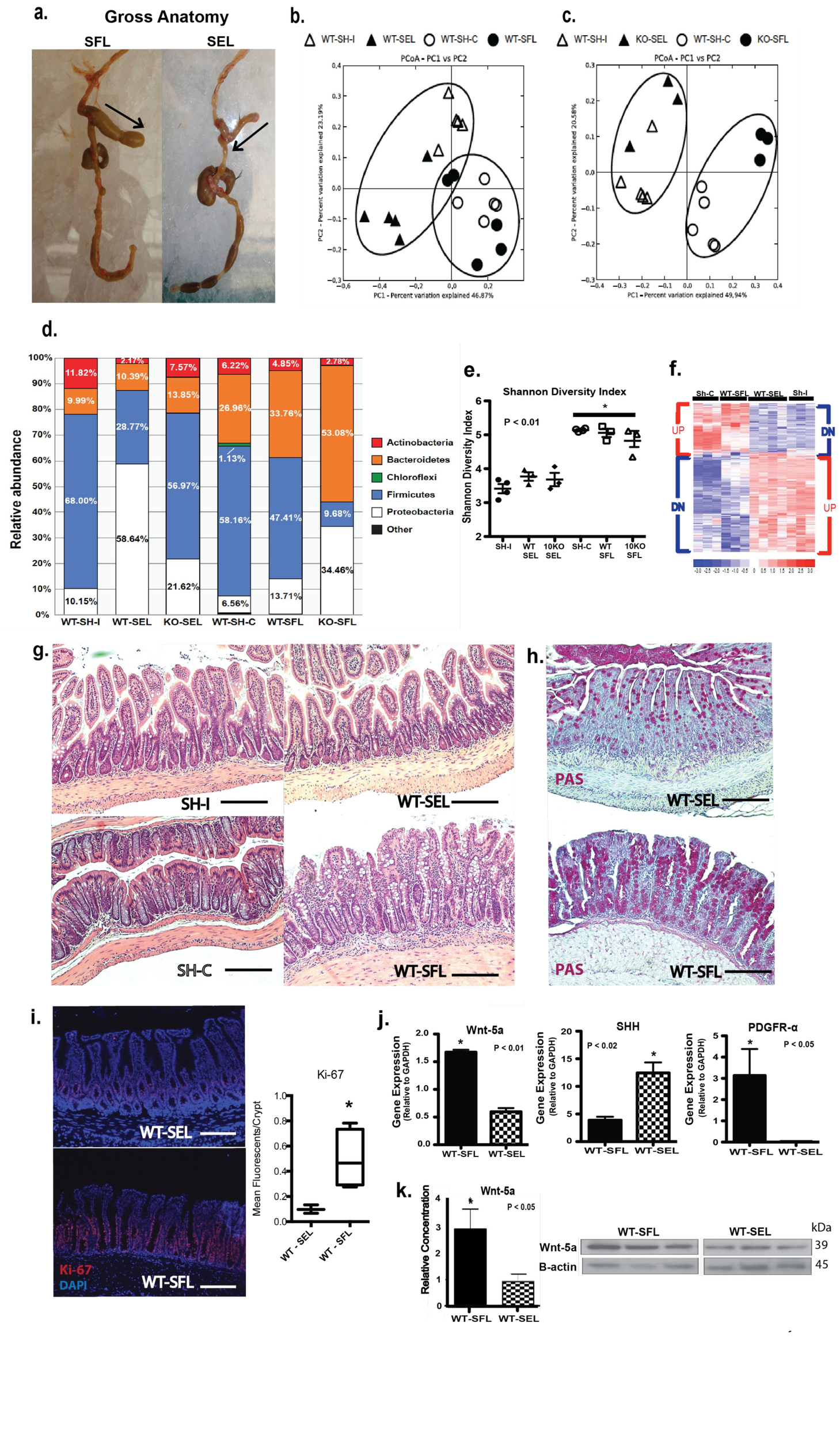
a.
Gross Anatomy
SFL
SEL
b.
WT-SH-I
WT-SEL
WT-SH-C
WT-SFL
PCoA - PC1 vs PC2
PC2 - Percent variation explained 23.19%
PC1 - Percent variation explained 46.87%
c.
WT-SH-I
KO-SEL
WT-SH-C
KO-SFL
PCoA - PC1 vs PC2
PC2 - Percent variation explained 20.58%
PC1 - Percent variation explained 49.94%
d.
Relative abundance
11.82%
9.99%
68.00%
10.15%
2.17%
10.39%
28.77%
58.64%
7.57%
13.85%
56.97%
21.62%
6.22%
26.96%
1.13%
58.16%
6.56%
4.85%
33.76%
47.41%
13.71%
2.78%
53.08%
9.68%
34.46%
WT-SH-I
WT-SEL
KO-SEL
WT-SH-C
WT-SFL
KO-SFL
Actinobacteria
Bacteroidetes
Chloroflexi
Firmicutes
Proteobacteria
Other
e.
Shannon Diversity Index
Shannon Diversity Index
P < 0.01
*
SH-I
WT SEL
10KO SEL
SH-C
WT SFL
10KO SFL
f.
Sh-C
WT-SFL
WT-SEL
Sh-I
UP
DN
DN
UP
g.
SH-I
WT-SEL
SH-C
WT-SFL
h.
PAS
WT-SEL
PAS
WT-SFL
i.
WT-SEL
Ki-67
DAPI
WT-SFL
Ki-67
Mean Fluorescents/Crypt
*
WT - SEL
WT - SFL
j.
Wnt-5a
P < 0.01
Gene Expression (Relative to GAPDH)
WT-SFL
WT-SEL
SHH
P < 0.02
WT-SFL
WT-SEL
PDGFR-α
P < 0.05
WT-SFL
WT-SEL
k.
Wnt-5a
P < 0.05
Relative Concentration
WT-SFL
WT-SEL
WT-SFL
WT-SEL
kDa
Wnt-5a
39
B-actin
45

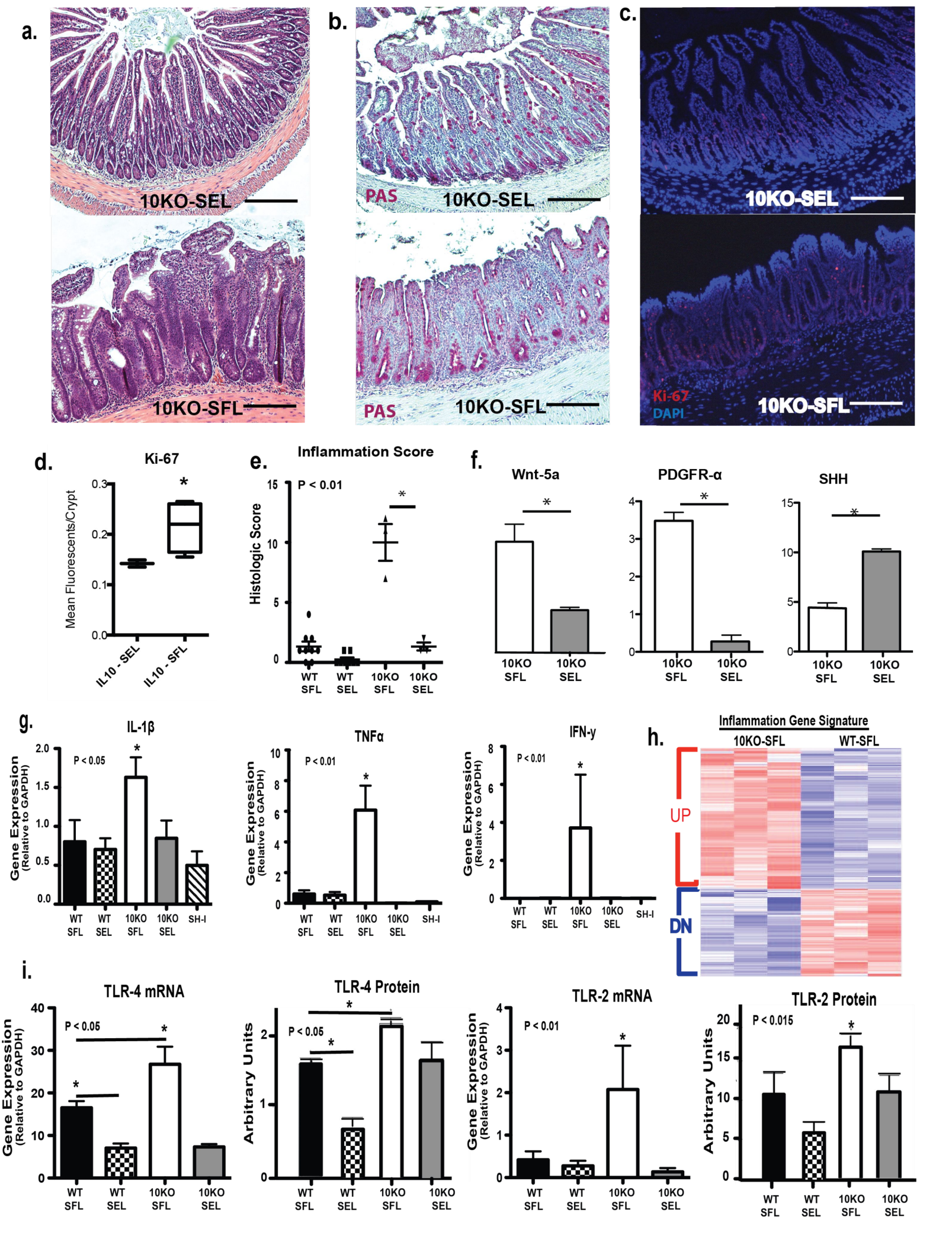
a.
10KO-SEL
10KO-SFL
b.
PAS
10KO-SEL
PAS
10KO-SFL
c.
10KO-SEL
Ki-67
DAPI
10KO-SFL
d.
Ki-67
Mean Fluorescents/Crypt
0.3
0.2
0.1
0.0
*
IL10 - SEL
IL10 - SFL
e.
Inflammation Score
P < 0.01
Histologic Score
15
10
5
0
*
WT SFL
WT SEL
10KO SFL
10KO SEL
f.
Wnt-5a
PDGFR-α
SHH
*
10KO SFL
10KO SEL
g.
IL-1β
P < 0.05
TNFα
P < 0.01
IFN-γ
P < 0.01
Gene Expression (Relative to GAPDH)
WT SFL
WT SEL
10KO SFL
10KO SEL
SH-I
h.
Inflammation Gene Signature
10KO-SFL
WT-SFL
UP
DN
i.
TLR-4 mRNA
P < 0.05
TLR-4 Protein
P < 0.05
TLR-2 mRNA
P < 0.01
TLR-2 Protein
P < 0.015
Arbitrary Units

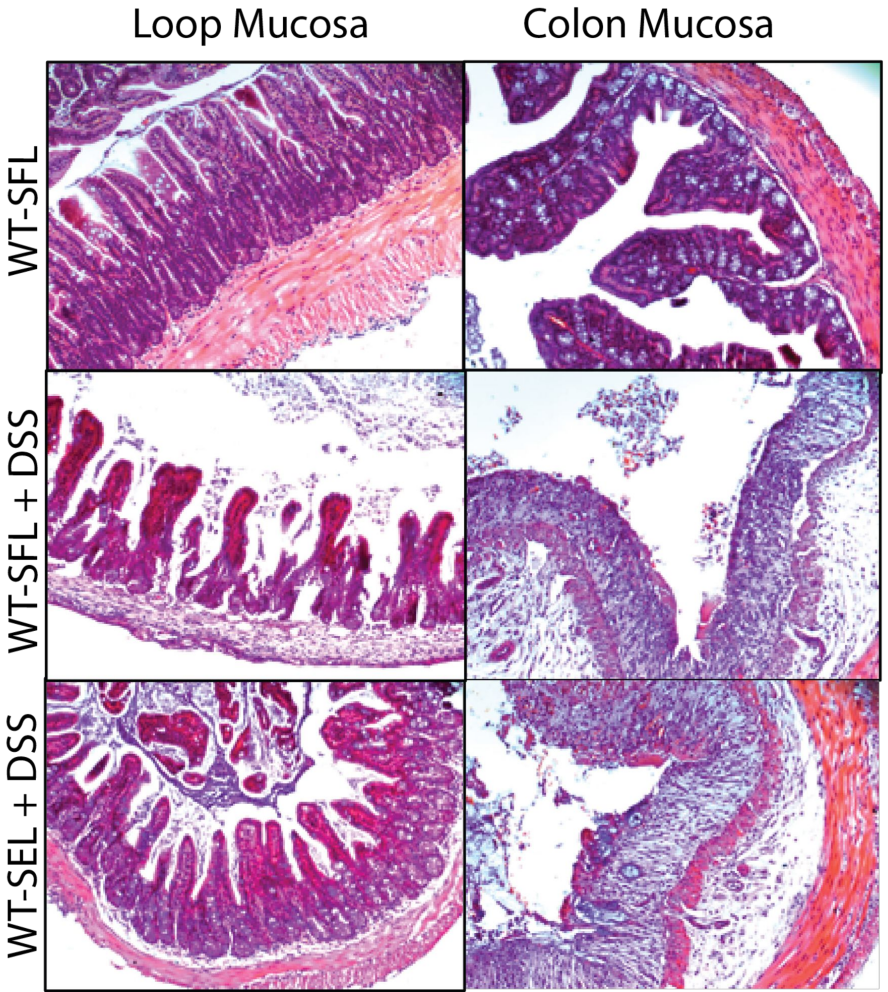
Loop Mucosa
Colon Mucosa
WT-SFL
WT-SFL + DSS
WT-SEL + DSS

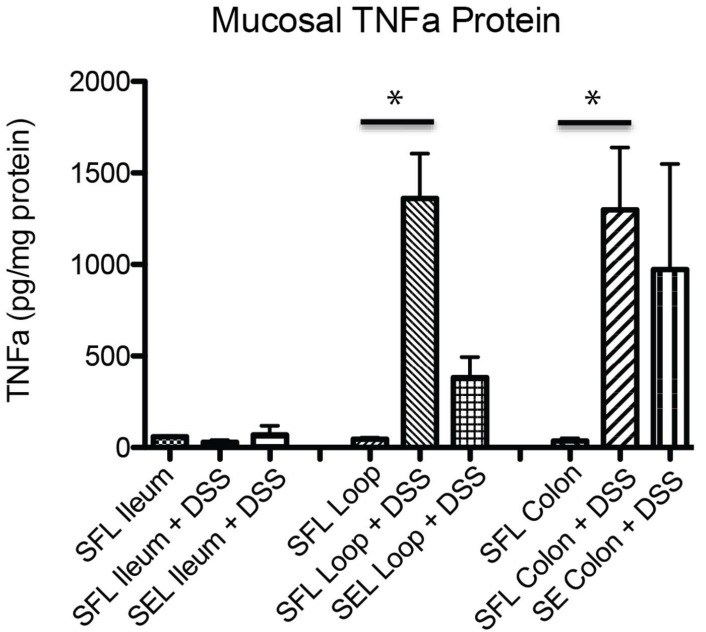
Mucosal TNFa Protein
TNFa (pg/mg protein)
2000
1500
1000
500
0
*
*
SFL Ileum
SFL Ileum + DSS
SEL Ileum + DSS
SFL Loop
SFL Loop + DSS
SEL Loop + DSS
SFL Colon
SFL Colon + DSS
SE Colon + DSS

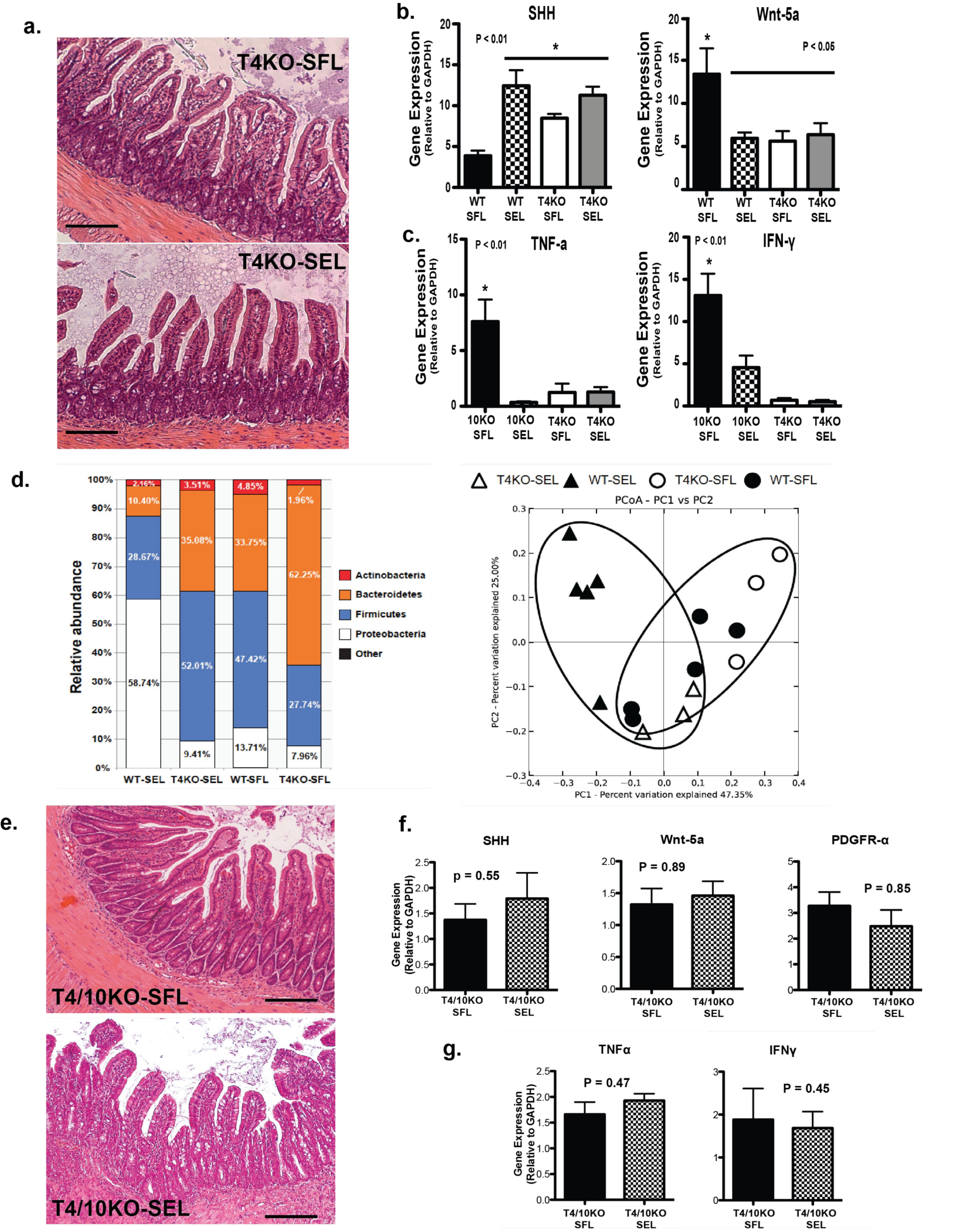
a.
T4KO-SFL
T4KO-SEL
b.
SHH
P < 0.01
*
Gene Expression (Relative to GAPDH)
WT SFL
WT SEL
T4KO SFL
T4KO SEL
Wnt-5a
*
P < 0.05
c.
TNF-a
P < 0.01
*
10KO SFL
10KO SEL
T4KO SFL
T4KO SEL
IFN-γ
P < 0.01
*
d.
Relative abundance
WT-SEL
T4KO-SEL
WT-SFL
T4KO-SFL
2.16%
10.40%
28.67%
58.74%
3.51%
35.08%
52.01%
9.41%
4.85%
33.75%
47.42%
13.71%
1.96%
62.25%
27.74%
7.96%
Actinobacteria
Bacteroidetes
Firmicutes
Proteobacteria
Other
T4KO-SEL
WT-SEL
T4KO-SFL
WT-SFL
PCoA - PC1 vs PC2
PC2 - Percent variation explained 25.00%
PC1 - Percent variation explained 47.35%
e.
T4/10KO-SFL
T4/10KO-SEL
f.
SHH
p = 0.55
Gene Expression (Relative to GAPDH)
T4/10KO SFL
T4/10KO SEL
Wnt-5a
P = 0.89
PDGFR-α
P = 0.85
g.
TNFα
P = 0.47
IFNγ
P = 0.45

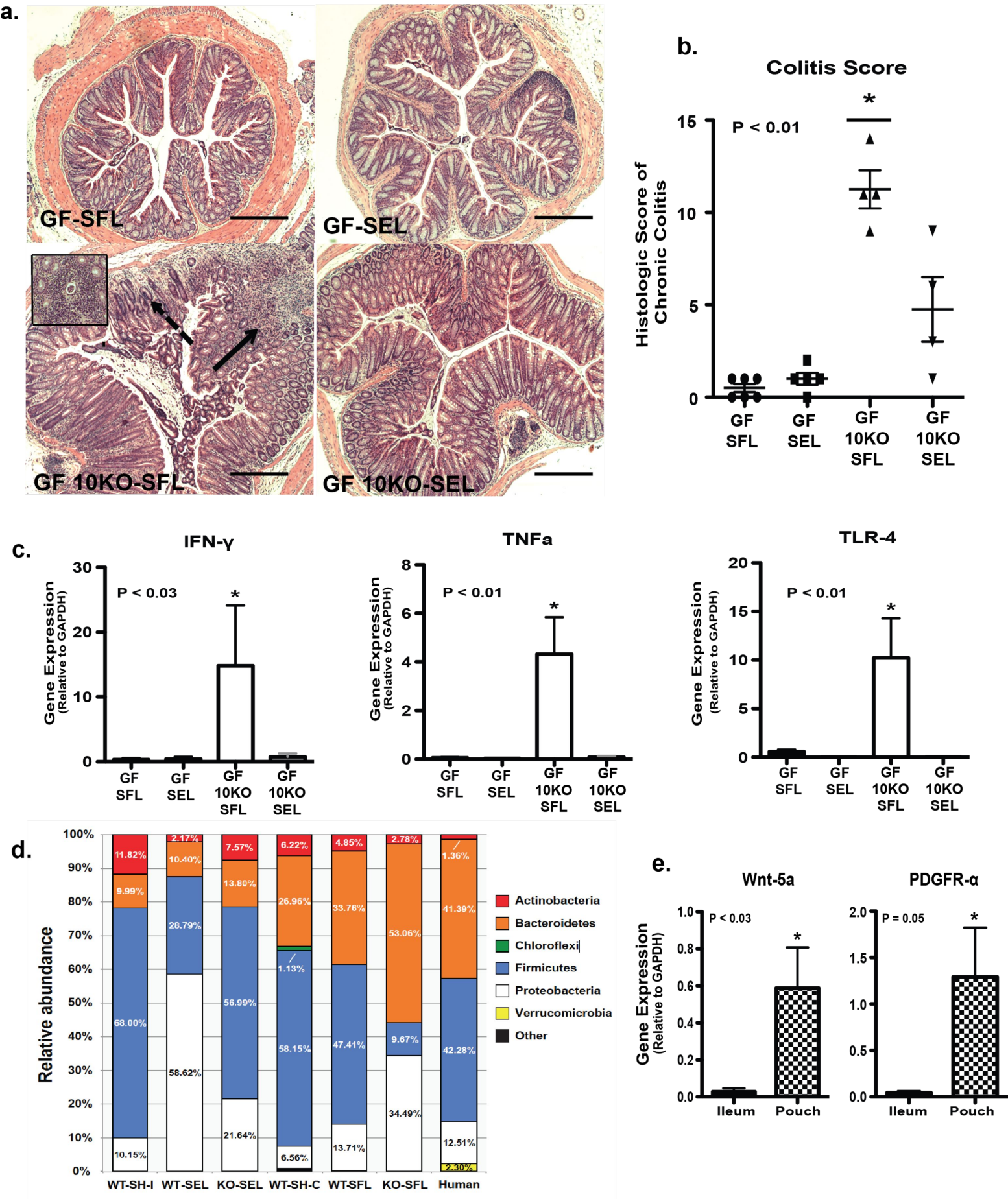
a.
GF-SFL
GF-SEL
GF 10KO-SFL
GF 10KO-SEL
b.
Colitis Score
P < 0.01
Histologic Score of Chronic Colitis
GF SFL
GF SEL
GF 10KO SFL
GF 10KO SEL
c.
IFN-γ
P < 0.03
TNFa
P < 0.01
TLR-4
P < 0.01
Gene Expression (Relative to GAPDH)
d.
Relative abundance
WT-SH-I
WT-SEL
KO-SEL
WT-SH-C
WT-SFL
KO-SFL
Human
Actinobacteria
Bacteroidetes
Chloroflexi
Firmicutes
Proteobacteria
Verrucomicrobia
Other
e.
Wnt-5a
P < 0.03
PDGFR-α
P = 0.05
Ileum
Pouch

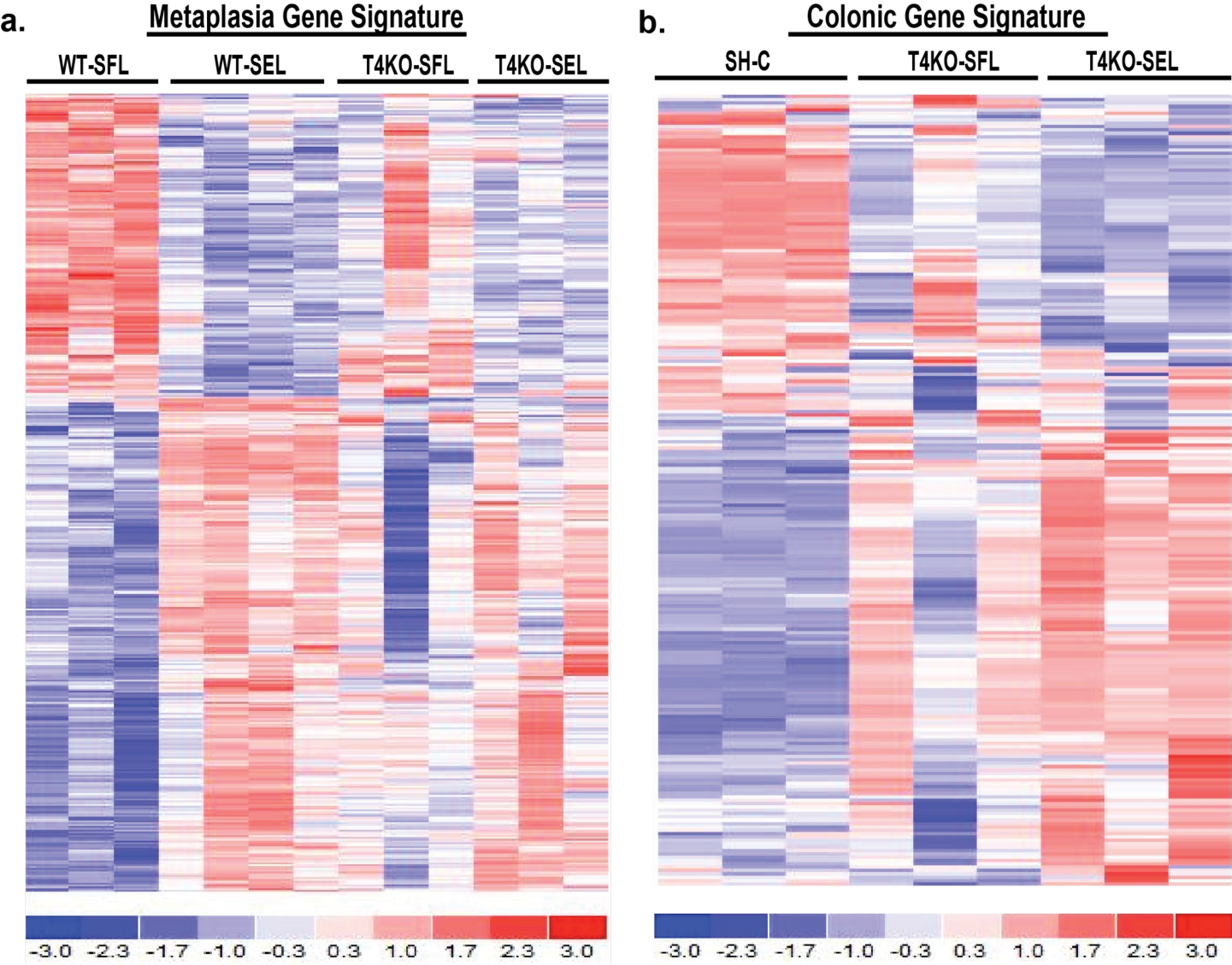
a.
Metaplasia Gene Signature
WT-SFL
WT-SEL
T4KO-SFL
T4KO-SEL
-3.0 -2.3 -1.7 -1.0 -0.3 0.3 1.0 1.7 2.3 3.0
b.
Colonic Gene Signature
SH-C
T4KO-SFL
T4KO-SEL
-3.0 -2.3 -1.7 -1.0 -0.3 0.3 1.0 1.7 2.3 3.0

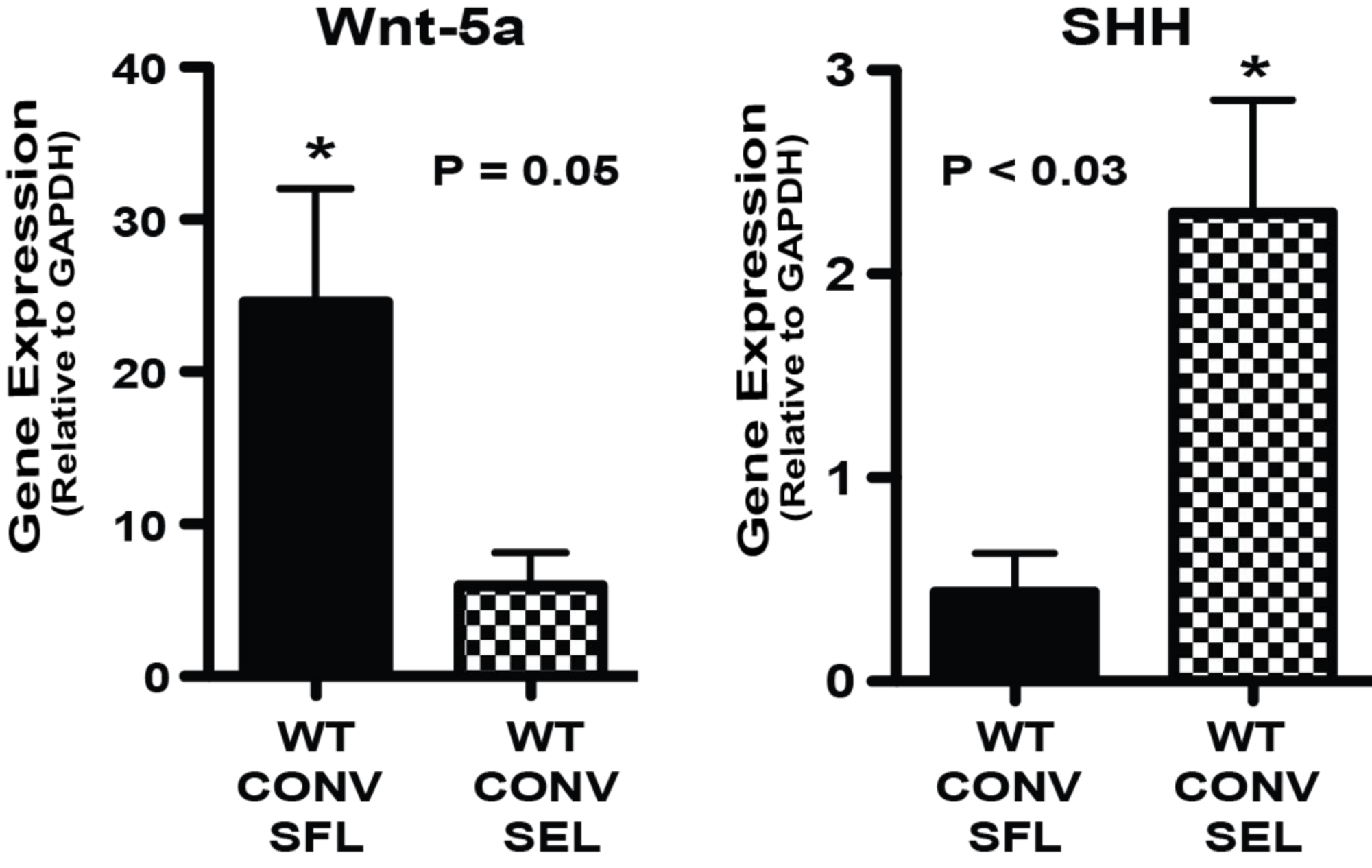
Wnt-5a
Gene Expression
(Relative to GAPDH)
40
30
20
10
0
*
P = 0.05
WT CONV SFL
WT CONV SEL
SHH
Gene Expression
(Relative to GAPDH)
3
2
1
0
*
P < 0.03
WT CONV SFL
WT CONV SEL

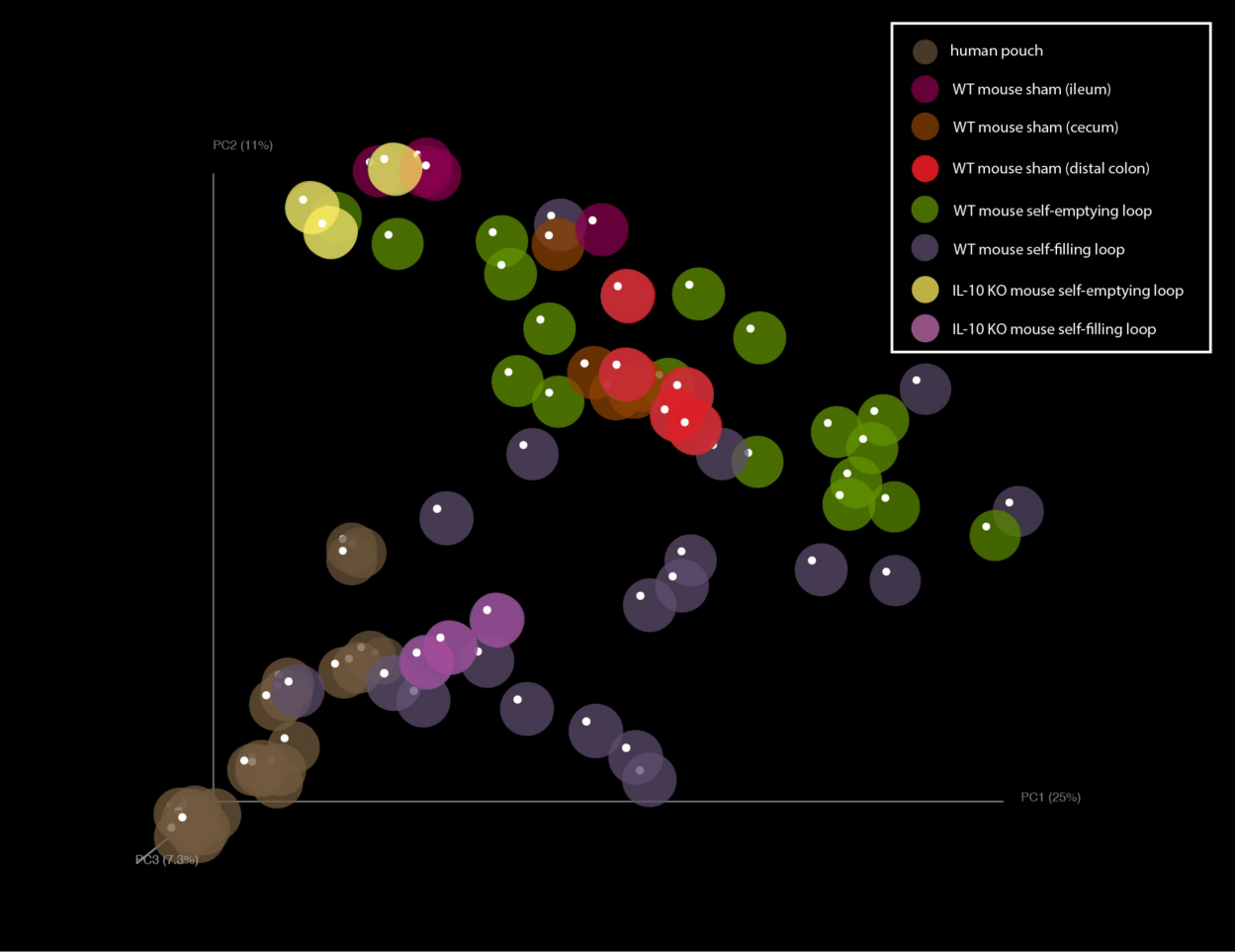
human pouch
WT mouse sham (ileum)
WT mouse sham (cecum)
WT mouse sham (distal colon)
WT mouse self-emptying loop
WT mouse self-filling loop
IL-10 KO mouse self-emptying loop
IL-10 KO mouse self-filling loop
PC2 (11%)
PC1 (25%)
PC3 (7.3%)

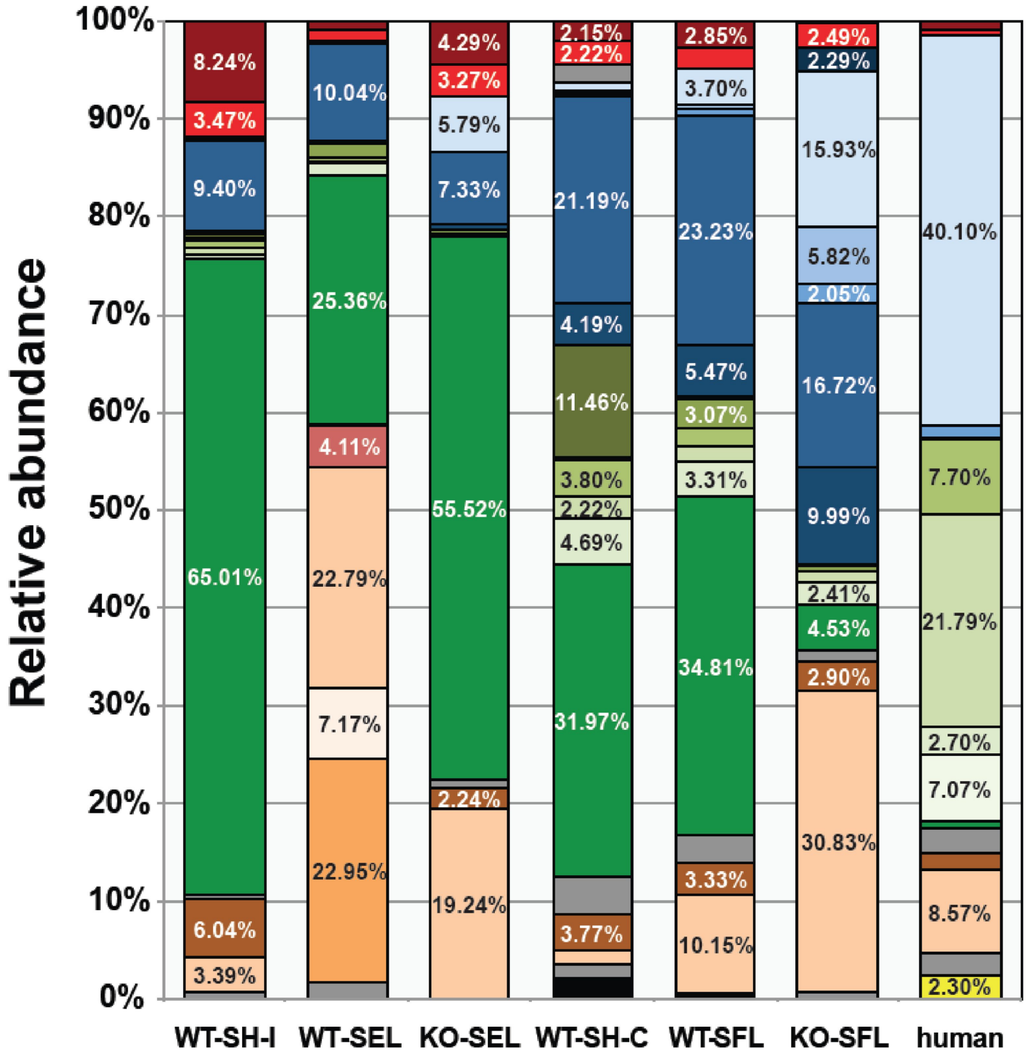

Actinobacteria

- cl. Actinobacteria; or. Bifidobacteriales; fa. *Bifidobacteriaceae*
- cl. Coriobacteriia; or. Coriobacteriales; fa. *Coriobacteriaceae*
- Other

Bacteroidetes

- cl. Bacteroidia;or. Bacteroidales;fa. not determined
- cl. Bacteroidia;or. Bacteroidales;fa. *Bacteroidaceae*
- cl. Bacteroidia;or. Bacteroidales;fa. *Porphyromonadaceae*
- cl. Bacteroidia;or. Bacteroidales;fa. *Rikenellaceae*
- cl. Bacteroidia;or. Bacteroidales;fa. *S24-7*
- cl. Bacteroidia;or. Bacteroidales;fa. [Paraprevotellaceae]
- Other

Firmicutes

- cl. Bacilli; or. Bacillales; fa. *Bacillaceae*
- cl. Bacilli; or. Lactobacillales; fa. *Lactobacillaceae*
- cl. Clostridia; or. Clostridiales; fa. not determined
- cl. Clostridia; or. Clostridiales; fa. *Lachnospiraceae*
- cl. Clostridia; or. Clostridiales; fa. *Ruminococcaceae*
- cl. Clostridia; or. Clostridiales; fa. *Veillonellaceae*
- cl. Erysipelotrichi; or. Erysipelotrichales; fa. *Erysipelotrichaceae*
- Other

Proteobacteria

- cl. Betaproteobacteria; or. Burkholderiales; fa. *Alcaligenaceae*
- cl. Betaproteobacteria; or. Burkholderiales; fa. *Comamonadaceae*
- cl. Gammaproteobacteria; or. Enterobacteriales; fa. *Enterobacteriaceae*
- cl. Gammaproteobacteria; or. Pseudomonadales; fa. *Moraxellaceae*
- cl. Gammaproteobacteria; or. Pseudomonadales; fa. *Pseudomonadaceae*
- Other

Verrucomicrobia

- cl. Verrucomicrobiae; or.Verrucomicrobiales; fa. *Verrucomicrobiaceae*
- Other

Other phyla

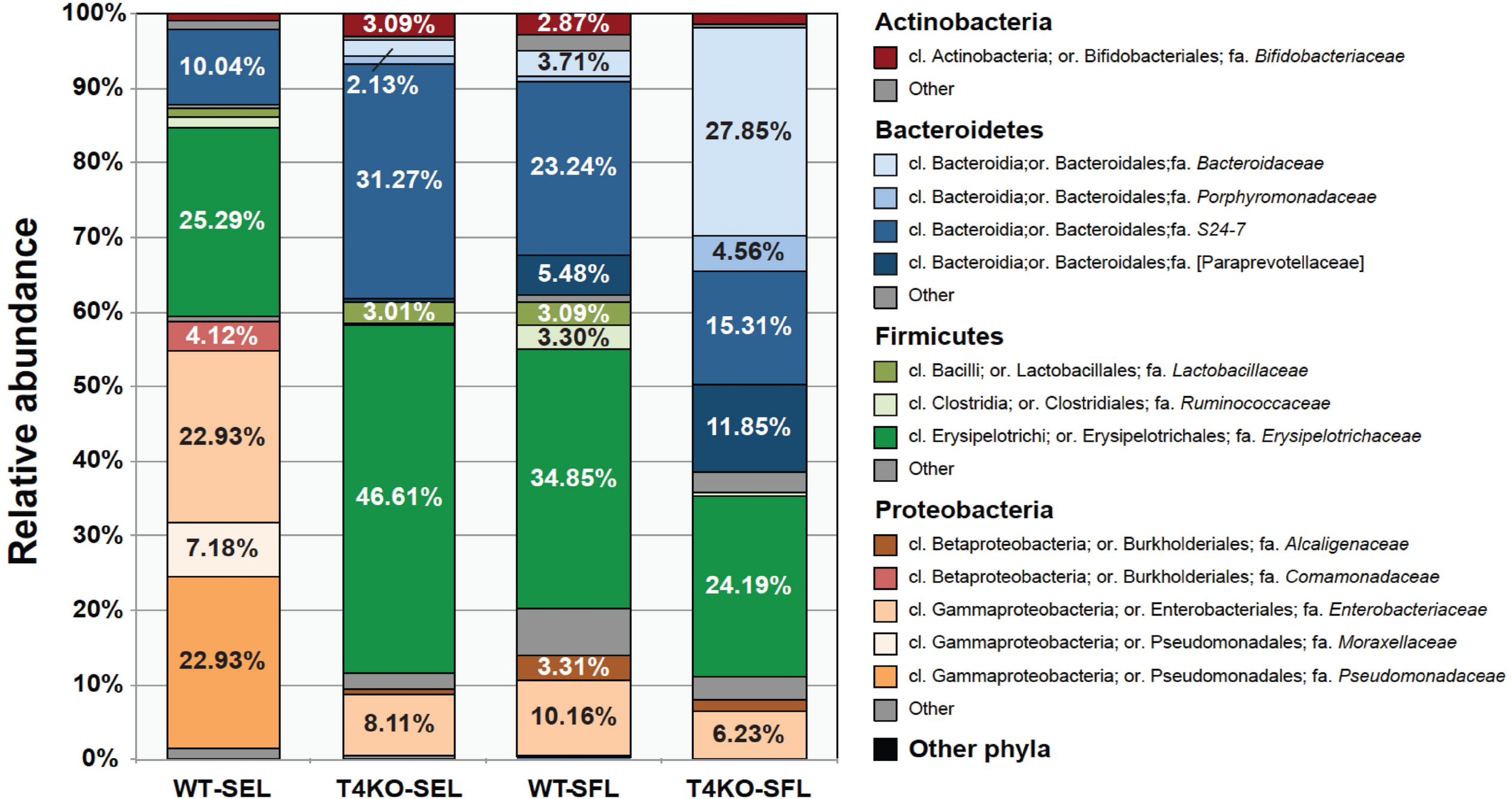
Relative abundance
100%
90%
80%
70%
60%
50%
40%
30%
20%
10%
0%
WT-SEL
T4KO-SEL
WT-SFL
T4KO-SFL
10.04%
25.29%
4.12%
22.93%
7.18%
22.93%
3.09%
2.13%
31.27%
3.01%
46.61%
8.11%
2.87%
3.71%
23.24%
5.48%
3.09%
3.30%
34.85%
3.31%
10.16%
27.85%
4.56%
15.31%
11.85%
24.19%
6.23%
Actinobacteria
cl. Actinobacteria; or. Bifidobacteriales; fa. Bifidobacteriaceae
Other
Bacteroidetes
cl. Bacteroidia;or. Bacteroidales;fa. Bacteroidaceae
cl. Bacteroidia;or. Bacteroidales;fa. Porphyromonadaceae
cl. Bacteroidia;or. Bacteroidales;fa. S24-7
cl. Bacteroidia;or. Bacteroidales;fa. [Paraprevotellaceae]
Other
Firmicutes
cl. Bacilli; or. Lactobacillales; fa. Lactobacillaceae
cl. Clostridia; or. Clostridiales; fa. Ruminococcaceae
cl. Erysipelotrichi; or. Erysipelotrichales; fa. Erysipelotrichaceae
Other
Proteobacteria
cl. Betaproteobacteria; or. Burkholderiales; fa. Alcaligenaceae
cl. Betaproteobacteria; or. Burkholderiales; fa. Comamonadaceae
cl. Gammaproteobacteria; or. Enterobacteriales; fa. Enterobacteriaceae
cl. Gammaproteobacteria; or. Pseudomonadales; fa. Moraxellaceae
cl. Gammaproteobacteria; or. Pseudomonadales; fa. Pseudomonadaceae
Other
Other phyla

Pathway Analysis of Colonic Gene Signature

Up-regulated	Down-Regulated
No significant Differences	Immune Response
	Antigen Processing and Presentation
	Cell Surface Receptor Linked Signal Transduction
	Proteolysis

Differentially Expressed Genes in Colonic Gene Signature

Gene	logFC	Gene	logFC	Gene	logFC	Gene	logFC	Gene	logFC	Gene	logFC
Muc4	1.05	Axud1	1.1	Hsd3b2	-2.03	Glipr2	-1.13	Rcan1	-1.61	Gpr114	-1.14
Agr2	1.24	Bhlhb2	1.17	EG665378	-1.61	Aqp7	-1.67	1700011H14Rik	-3.06	Ccl5	-1.93
Car9	1.1	Acsl3	1.14	Clk4	-1	Aqp7	-1.64	Cndp1	-1.33	Cd3g	-1.83
Nt5c2	1.17	Capn2	1.2	Slc38a2	-1.11	Tmem144	-1.18	Slc5a11	-1.95	Cd3d	-1.3
Steap1	1	Capn2	1.13	Snapc3	-1.06	Rdh7	-1.81	Abp1	-1.17	Ctsw	-1.86
EG433182	1.02	Capn2	1.17	Gnpda1	-1.41	Rdh7	-1.75	Akr1b7	-2.36	Itgae	-1.29
Kremen2	1.12	Ranbp1	1.01	Gnpda1	-1.18	Taf4a	-1.73	1200009I06Rik	-1.22	Itgae	-1.27
Clic1	1.18	Il1rn	1.73	Cd8b1	-1.23	H2-Aa	-1.37	Mme	-1.07	Nkg7	-1.44
Chst4	1.34	B3galt5	2	Enpp7	-2.78	H2-Ab1	-1.57	Slc7a15	-1.27	Cd3e	-1.39
Lmna	1.11	Hsd11b2	1.12	Enpp7	-2.29	H2-Ab1	-1.39	Slc47a1	-1.21	Gbp3	-1.22
Lmna	1.24	B3gnt7	1.17	Hoxb4	-1.07	H2-Ab1	-1.64	1300013J15Rik	-1.04	Ppap2b	-1.26
Lmna	1.03	Anxa3	1.1	Angptl1	-1.13	LOC641240	-1.44	Xpnpep2	-1.48	Aif1	-1.11
Lmna	1.15	Anxa3	1.18	Es1	-1.26	Aqp1	-1.04	Tmem86b	-1.24	Gucy1a3	-1.05
Hif1a	1.77	Blnk	1.07	Hoxc6	-1.45	Tmem86a	-1.25	Mme	-1.63	BC034076	-1.72
Tmsb10	1.07	Srd5a2	1.66	Tgfbi	-1.42	H2-DMa	-1.16	1300013J15Rik	-1.88	Itga11	-1.45
Lamc2	1.18	Klk1	1.49	Tgfbi	-1.09	Ang	-1.14	Sesn1	-1.05	Itpr2	-1.15
Evi1	1.3	Klk1b5	1.47	Dab1	-1.59	Susd2	-1.73	Fam118a	-1.01	Gimap8	-1.08
1700019H03Rik	1.52	Klk1b4	1.33	Dab1	-1.46	Slc15a1	-1.24	Cyp4b1	-1.89	Vapb	-1.19
Fam162a	1.58	Klk1b27	1.53	Cfl2	-2.14	Mapk4	-1.05	Rnf208	-1.45	Ephx2	-1.86
Dmbt1	1.16	B3gnt5	1.5	Habp2	-1.1	Bmp1	-1.93	Mycbpap	-1.3	Cyp2d26	-2.28
Gstk1	1.34	Pla2g10	1.41	Khk	-1	Ace	-1.44	Casp4	-1.18	Cyp2d26	-2.24
Gjb3	1.17	Ela1	1.46	Slc7a9	-1.13	Chst8	-1.6	Klrd1	-1.02	Cyp2d26	-2.21
Akr1b8	2.55	Slc45a3	1.55	Defa1	-2.12	Ace	-1.28	LOC100047214	-1.06	Krba1	-1.15
Lgals3	1.01	Ildr1	1.42	Guca2b	-1.04	Bmp1	-1.07	Vps33b	-1.1	Cat	-1.42
Mboat1	2.2	Ildr1	1.55	Prkg2	-1.23	Relb	-1.14	Vps33b	-1	Krba1	-1.22
S100a16	1.33	Gna14	1.51	Defa1	-1.02	Ttc36	-1.94	Lcp1	-1.01	Rnf167	-1.28
S100a14	2.12	Tspan1	1.31	Defcr21	-1.39	Bmp1	-1.08	Ghr	-1.31	H2-T23	-1.08
Ankrd22	1.09	Aqp4	1.52	Naaladl1	-1.09	Iyd	-1.26	5730469M10Rik	-1.45	Rnf167	-1.25
ORF9	1.14	Car4	1.08	Naaladl1	-1.28	Rnase4	-1.42	Ghr	-1.22	Rnf167	-1.43
Apobec1	1	Slc2a1	1.43	Naaladl1	-1.16	Gal3st2	-1.13	Lpl	-3.18	Irf9	-1.18
Gprc5a	2.67	Agpat4	1.01	Habp2	-1.19	C2	-1.45	Myl1	-2.08	Sepp1	-2.13
Gusb	1.02	Pik3r3	1.04	Habp2	-1.14	Slc5a4b	-1.25	Ppp1r1a	-1.69	Sepp1	-1.78
2610209A20Rik	1.05	Ly6a	1.76	Ugt2b36	-1.16	G6pc	-2.34	Rnf144a	-1.24	Dnase1l3	-1.12
Hddc2	1.03	Acot7	1.02	1200009I06Rik	-1.16	Mep1a	-1.45	Cfd	-5.46	Abi3bp	-1.63
Pqlc3	1.22	Acot7	1.05	Amn	-1.33	Rnf128	-1.21	Cldn10	-1.33	Taf15	-1.61
Pqlc3	1.32	Fos	2.27	Ugt2b36	-1.19	Sesn1	-1.45	Bex4	-1.2	Hoxb5	-1.27
Igfbp2	2.1	Areg	2.2	Pepd	-1.08	Tyki	-1.7	Cd160	-1.02	Oasl2	-1
Igfbp2	2.57	Fkbp5	1.11	Pdzk1	-2.59	Slc16a10	-1.4	H2-Eb1	-1.63	Rsad2	-1.75
Plk3	1.3	Eva1	1.3	Xpnpep2	-1.75	Gdpd2	-1.04	Rasgrp1	-1.1	Oasl2	-1.53
						Cyp4v3	-2.05	Lck	-1		

a.

Metaplastic Gene Signature

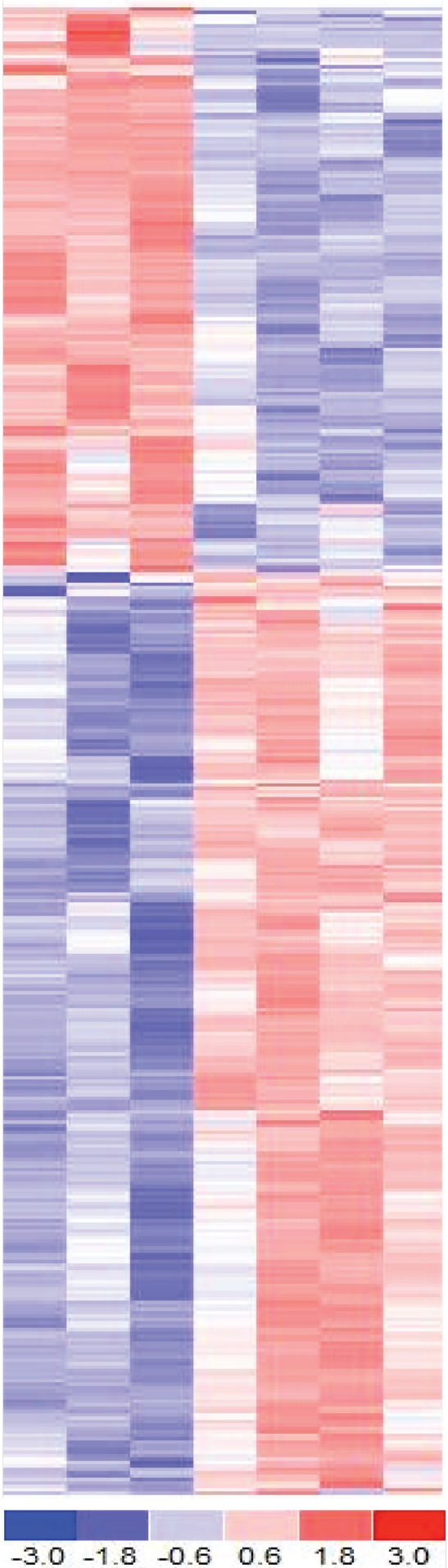

b.

Differentially Expressed Genes in Metaplastic Gene Signature

Gene	logFC	Gene	logFC	Gene	logFC	Gene	logFC	Gene	logFC	Gene	logFC
Steap1	1	Asns	1.29	Igfbp2	2.57	Aatk	-1.52	Tmem86a	-1.25	Hoxb4	-1.07
Apobec1	1	Lypd3	1.29	Gprc5a	2.67	D12Ertd647e	-1.51	Slc5a4b	-1.25	Qpct	-1.07
Sphk1	1	Evi1	1.3	Ly6d	2.7	Rtn1	-1.51	Tmem86b	-1.24	Rgs10	-1.07
Lgals3	1.01	Eva1	1.3	Lrg1	2.8	Sdpr	-1.5	Slc15a1	-1.24	Chrm2	-1.07
Ranbp1	1.01	Plk3	1.3	Ly6d	3.15	Plscr4	-1.49	Rnf144a	-1.24	LOC100047214	-1.06
Agpat4	1.01	G630016D24Rik	1.31	LOC100043836	3.66	Fbxo32	-1.49	Prkg2	-1.23	Fgf13	-1.06
Tmem139	1.01	Tspan1	1.31	Cfd	-5.46	Slc5a6	-1.49	Cd8b1	-1.23	Snapc3	-1.06
S100a11	1.02	Il33	1.31	Lpl	-3.18	Xpnpep2	-1.48	Eef1a2	-1.23	Mapk4	-1.05
Acot7	1.02	Pqlc3	1.32	1700011H14Rik	-3.06	Tnxb	-1.48	Krba1	-1.22	Gucy1a3	-1.05
Gusb	1.02	S100a16	1.33	Ces3	-3.02	Dab1	-1.46	Ghr	-1.22	Sesn1	-1.05
EG433182	1.02	Klk1b4	1.33	Enpp7	-2.78	D12Ertd647e	-1.45	Cytip	-1.22	Cdkn1c	-1.05
Tm4sf4	1.02	Gstk1	1.34	Pdzk1	-2.59	Mep1a	-1.45	Gbp3	-1.22	Tshz3	-1.05
Slc16a6	1.02	Chst4	1.34	Akr1b7	-2.36	Sesn1	-1.45	Adh1	-1.22	Guca2b	-1.04
Lmna	1.03	Tmsb10	1.36	G6pc	-2.34	Rnf208	-1.45	1200009I06Rik	-1.22	Gdpd2	-1.04
Srd5a1	1.03	Tfrc	1.36	Dio1	-2.33	Itga11	-1.45	Cldn5	-1.22	1300013J15Rik	-1.04
Hddc2	1.03	Ttyh1	1.36	Olfr165	-2.32	C2	-1.45	Slc47a1	-1.21	Gstt1	-1.04
Smox	1.03	Plaur	1.39	Enpp7	-2.29	5730469M10Rik	-1.45	Rnf128	-1.21	Gcnt1	-1.04
Asns	1.04	Mlp	1.4	Cyp2d26	-2.28	Tnxb	-1.45	Cyp27a1	-1.21	Aqp1	-1.04
Pik3r3	1.04	Pla2g10	1.41	Cyp2d26	-2.24	Hoxc6	-1.45	Bex4	-1.2	Cugbp2	-1.04
Cd44	1.04	Tfrc	1.41	Cyp2d26	-2.21	Ace	-1.44	Ptprb	-1.2	Kcnf1	-1.04
Acot7	1.05	Sprr1a	1.41	Trpm6	-2.18	Nkg7	-1.44	Mettl7b	-1.2	Nav1	-1.03
Prkaa2	1.05	9830002I17Rik	1.42	Cfl2	-2.14	Ndn	-1.44	Vapb	-1.19	Il17re	-1.02
Por	1.05	Ildr1	1.42	Sepp1	-2.13	LOC641240	-1.44	Habp2	-1.19	Cd160	-1.02
2610209A20Rik	1.05	Fgf15	1.42	Defa1	-2.12	Rnf167	-1.43	Ugt2b36	-1.19	Defa1	-1.02
Muc4	1.05	Fkbp11	1.43	Myl1	-2.08	Neu1	-1.42	Casp4	-1.18	6330403K07Rik	-1.02
Btc	1.06	Slc2a1	1.43	Cyp4v3	-2.05	Cat	-1.42	Irf9	-1.18	Klrd1	-1.02
Spdef	1.06	Marcksl1	1.43	Sectm1b	-2.05	Rnase4	-1.42	Tmem144	-1.18	Lcp1	-1.01
Tmsb10	1.07	Ela1	1.46	Hsd3b2	-2.03	Tgfbi	-1.42	Prkacb	-1.18	Fam118a	-1.01
Blnk	1.07	BC067047	1.46	H2-M2	-1.96	Rgma	-1.42	Gnpda1	-1.18	Tmem25	-1
Car4	1.08	Gch1	1.46	Slc5a11	-1.95	Mrvi1	-1.42	Rasl11b	-1.18	3632451O06Rik	-1
Car9	1.09	Klk1b5	1.47	Ttc36	-1.94	Gnpda1	-1.41	Abp1	-1.17	Lck	-1
Entpd7	1.09	Tm4sf4	1.47	Bmp1	-1.93	Gucy1a3	-1.41	Naaladl1	-1.16	Vps33b	-1
Ankrd22	1.09	Klk1	1.49	Ccl5	-1.93	Slc16a10	-1.4	Gas6	-1.16	Oasl2	-1
Mt3	1.09	B3gnt5	1.5	LOC100045005	-1.89	Fbxo32	-1.4	1200009I06Rik	-1.16	Khk	-1
Nptx2	1.1	2010109I03Rik	1.5	Cyp4b1	-1.89	Cd3e	-1.39	Ugt2b36	-1.16	4933428G20Rik	-1
Car9	1.1	Errfi1	1.51	Dio1	-1.88	Defcr21	-1.39	Wasf1	-1.16	Sh3kbp1	-1
Axud1	1.1	Gna14	1.51	1300013J15Rik	-1.88	H2-Ab1	-1.39	H2-DMa	-1.16	Clk4	-1
Anxa3	1.1	1700019H03Rik	1.52	Ctsw	-1.86	Cyp27a1	-1.37	Tgfbr3	-1.16		
Lmna	1.11	Aqp4	1.52	Ephx2	-1.86	H2-Aa	-1.37	Vapb	-1.15		
Tmsb10	1.11	Klk1b27	1.53	Ltbp4	-1.85	Robo4	-1.37	Krba1	-1.15		
Cldn4	1.11	Phlda1	1.54	Cd3g	-1.83	Ypel3	-1.36	Itpr2	-1.15		
Smox	1.11	Slc45a3	1.55	Rdh7	-1.81	Pdzrn3	-1.35	C4bp	-1.15		
Fkbp5	1.11	Ildr1	1.55	Sepp1	-1.78	Stmn2	-1.35	Gabarapl1	-1.15		
Kremen2	1.12	Egln3	1.56	Bex4	-1.77	Cndp1	-1.33	Rtn1	-1.15		
Hsd11b2	1.12	Prss27	1.57	Calb2	-1.77	D0H4S114	-1.33	Relb	-1.14		
2310005P05Rik	1.13	Fam162a	1.58	Rsad2	-1.75	Hpgd	-1.33	Ang	-1.14		
Capn2	1.13	Mfsd2	1.65	Xpnpep2	-1.75	Amn	-1.33	Habp2	-1.14		
ORF9	1.14	Srd5a2	1.66	Rdh7	-1.75	Igsf4a	-1.33	Gpr114	-1.14		
Acsl3	1.14	LOC100044256	1.69	Gdf10	-1.75	Fmo1	-1.33	LOC100045981	-1.14		
Rrm2	1.14	Cck	1.72	Taf4a	-1.73	Cldn10	-1.33	Slc7a9	-1.13		
Lmna	1.15	Il1rn	1.73	Susd2	-1.73	Igf2	-1.32	Hap1	-1.13		
Por	1.15	Tcf23	1.74	Hdac5	-1.72	Cyp27a1	-1.32	Angptl1	-1.13		
Dmbt1	1.16	Ly6a	1.76	BC034076	-1.72	Adh1	-1.32	Glipr2	-1.13		
Tnfrsf22	1.16	Hif1a	1.77	Nrp1	-1.71	Wwc2	-1.31	Gal3st2	-1.13		
Rpl38	1.16	2210407C18Rik	1.8	Tyki	-1.7	Mgll	-1.31	Ddx26b	-1.12		
Gjb3	1.17	E130012A19Rik	1.82	Ppp1r1a	-1.69	Ghr	-1.31	Vamp4	-1.12		
Bhlhb2	1.17	Chac1	1.86	Trpm6	-1.68	Reln	-1.31	Dnase1l3	-1.12		
Capn2	1.17	Cartpt	1.88	Akap12	-1.68	BC031353	-1.3	Ldb2	-1.12		
Prl2c4	1.17	S100a8	1.96	Aqp7	-1.67	Cd3d	-1.3	Slc25a36	-1.11		
Prl2c3	1.17	Plek2	1.99	Ltbp4	-1.67	Unc84b	-1.3	Plekhb1	-1.11		
Nt5c2	1.17	B3galt5	2	Edn1	-1.67	Mycbpap	-1.3	Slc38a2	-1.11		
B3gnt7	1.17	Tnfrsf12a	2.04	Neurl	-1.66	Rbms3	-1.3	Aif1	-1.11		
Clic1	1.18	Gsta1	2.04	Mustn1	-1.66	Zcchc18	-1.3	Habp2	-1.1		
Lamc2	1.18	Myl7	2.06	Sult1a1	-1.66	Itgae	-1.29	Vps33b	-1.1		
Anxa3	1.18	Krt84	2.07	Aqp7	-1.64	Meis2	-1.29	Hist1h1c	-1.1		
Capn2	1.2	Igfbp2	2.1	Rgs7bp	-1.64	Ace	-1.28	Rasgrp1	-1.1		
Tmc7	1.2	Gch1	2.11	H2-Ab1	-1.64	Rnf167	-1.28	Cav2	-1.1		
Fosb	1.2	Prss27	2.11	Tnxb	-1.64	Naaladl1	-1.28	Pecam1	-1.1		
Pqlc3	1.22	S100a14	2.12	Abi3bp	-1.63	Lmo2	-1.28	Il17re	-1.09		
Ripk3	1.22	Prss27	2.18	H2-Eb1	-1.63	Hoxb5	-1.27	Naaladl1	-1.09		
Lpcat4	1.22	Mboat1	2.2	Mme	-1.63	Itgae	-1.27	Magee1	-1.09		
Abpb	1.23	Ptpro	2.2	Rcan1	-1.61	Slc7a15	-1.27	Tgfbi	-1.09		
Lmna	1.24	Areg	2.2	EG665378	-1.61	Es1	-1.26	H2-T23	-1.08		
Agr2	1.24	Hbegf	2.23	Taf15	-1.61	Gcnt1	-1.26	Ppargc1a	-1.08		
Kcnk10	1.25	Fos	2.27	Chst8	-1.6	Iyd	-1.26	Bmp1	-1.08		
Rbp2	1.25	Phlda2	2.29	Maob	-1.59	Dusp26	-1.26	Gimap8	-1.08		
Sfn	1.26	Capg	2.32	Dab1	-1.59	Ppap2b	-1.26	Cyp2d10	-1.08		
Dppa3	1.27	Gsta2	2.48	H2-Ab1	-1.57	Cd1d1	-1.26	Pepd	-1.08		
Marcksl1	1.27	Cart	2.52	Cyp2d22	-1.53	Hdac5	-1.25	Bmp1	-1.07		
Pibf1	1.28	Akr1b8	2.55	Oasl2	-1.53	Rnf167	-1.25	Mme	-1.07		

Pathway Analysis Between KO Filling & Emptying Loops by Gene Array

Up-regulated	Down-regulated
immune response	No Significant Differences
inflammatory response	
positive regulation of phagocytosis	

Pathway Analysis Between KO & WT Filling Loops by Gene Array

Up-regulated	Down-regulated
response to cytokine stimulus	transcription
immunoglobulin mediated immune response	regulation of transcription, DNA-dependent
regulation of protein amino acid phosphorylation	G-protein coupled receptor protein signaling pathway
negative thymic T cell selection	oxidation reduction
defense response to Gram-positive bacterium	signal transduction
positive regulation of interleukin-6 production	
antigen processing and presentation of peptide or polysaccharide antigen via MHC class II	
antigen processing and presentation	
complement activation, classical pathway	
G-protein coupled receptor protein signaling pathway	
defense response to bacterium	
positive regulation of phagocytosis	
positive thymic T cell selection	
positive regulation of tumor necrosis factor production	
regulation of immune response	
innate immune response	
mast cell activation	
response to lipopolysaccharide	
defense response	
antigen processing and presentation of exogenous peptide antigen via MHC class II	
inflammatory response	
neutrophil chemotaxis	
chemotaxis	
phagocytosis, engulfment	
immune response	
cell surface receptor linked signal transduction	

Differentially Expressed Genes in Inflammation Gene Signature

Gene	logFC	Gene	logFC	Gene	logFC	Gene	logFC	Gene	logFC	Gene	logFC	Gene	logFC	Gene	logFC
Aoah	1	Vldlr	1.18	Tap2	1.49	1300007L22Rik	1.83	Gcnt1	2.53	Defb37	-2.15	Sri	-1.3	Slc22a1	-1.06
Arl11	1	Clec4n	1.18	H2-Ab1	1.49	Sirpb1	1.84	Slfn2	2.54	Cd55	-2.12	Ube2n	-1.29	Tmbim1	-1.06
Dpep2	1	BC028528	1.18	Timp3	1.49	Stfa2	1.84	H2-T10	2.55	AU018778	-2.12	Dab1	-1.29	Khk	-1.06
Trafd1	1	Gm2a	1.18	Cirbp	1.49	2210407C18Rik	1.84	B3galt5	2.55	Ihh	-2.06	Pccb	-1.28	Sema3b	-1.05
Cpne8	1	Darc	1.18	H2-Q7	1.5	Il18r1	1.85	Nkg7	2.58	Cops8	-2.04	Dsp	-1.28	Decr1	-1.05
LOC100044190	1	Itgae	1.18	H6pd	1.5	Ccr5	1.86	LOC100048346	2.6	Krt84	-2.03	Mrpl15	-1.28	Acbd4	-1.05
Hoxb5	1	BC028528	1.19	Spata6	1.51	Selplg	1.86	Cd3d	2.63	Rdh7	-2.01	Rapgefl1	-1.28	Camk1d	-1.05
EG432555	1	Arhgap30	1.19	Psmb9	1.51	Indo	1.88	Tap1	2.67	Dio1	-2	Oat	-1.27	Sema5a	-1.05
Slc1a5	1	Irf9	1.2	LOC435565	1.52	Adssl1	1.88	Upp1	2.68	Tmem117	-1.96	Gpr89	-1.27	Acvr1c	-1.05
Asah3l	1	Stat1	1.2	Flot2	1.52	Tnfaip2	1.89	Upp1	2.68	Tinag	-1.94	Tcf23	-1.27	Yme1l1	-1.05
Hk3	1.01	Elk3	1.2	Slc2a6	1.52	Rgs1	1.89	Fcer1g	2.69	Cyp4f16	-1.94	AI427809	-1.27	Defa1	-1.05
Casp4	1.01	Fermt3	1.21	Stat1	1.52	Ccl3	1.9	Myot	2.71	Gsta4	-1.93	LOC100045403	-1.27	Ccl27	-1.05
Fas	1.01	Vldlr	1.21	Fgf15	1.52	Sirpa	1.9	Tnfaip2	2.71	Aqp7	-1.91	Abpb	-1.26	Enpp7	-1.05
Map3k8	1.01	Pmaip1	1.21	EG433016	1.53	Cfl1	1.92	Fxyd5	2.72	1810023F06Rik	-1.91	Rras2	-1.26	Slc22a1	-1.04
Myd116	1.02	2610027C15Rik	1.21	H2-DMb1	1.53	Hdc	1.92	Il10	2.78	Fosb	-1.89	Esd	-1.26	Adk	-1.04
Chrd	1.02	LOC547343	1.22	Cyp3a13	1.53	Cd3e	1.93	C1qb	2.78	Defcr21	-1.89	Tspan3	-1.26	Pccb	-1.04
Arap1	1.02	Myo1f	1.22	Irf1	1.54	Coro1a	1.94	Tnf	2.79	Cth	-1.88	Ugt2b34	-1.25	Snx7	-1.04
Dok2	1.02	Zc3h12a	1.22	Ciita	1.54	Cd6	1.95	Ctse	2.8	Cyp4f16	-1.87	Immp2l	-1.24	Lrrc50	-1.04
Herpud1	1.03	Xdh	1.23	Cd74	1.54	Cd177	1.95	AI451557	2.81	Cps1	-1.83	Eef1d	-1.24	Als2	-1.04
Fxyd5	1.03	Gbp10	1.23	LOC100041504	1.54	0610010D20Rik	1.95	OTTMUSG00000000971	2.81	Scin	-1.83	Lace1	-1.24	Tsc22d1	-1.04
Srgn	1.03	Gpr171	1.23	Ccrl2	1.55	Vcam1	1.95	Retnlg	2.85	Adcy8	-1.82	Syt12	-1.23	8430419L09Rik	-1.03
Stat4	1.03	Wars	1.24	Flot2	1.55	Sema6b	1.96	1600029D21Rik	2.86	Otc	-1.81	Hr	-1.23	Cyp4f14	-1.03
Ildr1	1.03	1-Mar	1.24	Slamf8	1.55	Expi	1.96	Gbp3	2.89	Prmt2	-1.8	Rtkn	-1.22	Rhod	-1.03
Pla1a	1.03	H2-Q2	1.25	Cyp1b1	1.55	Serping1	1.96	Iigp2	2.9	Cox7a1	-1.79	Gamt	-1.22	Sord	-1.03
Trim40	1.03	Epb7.2	1.25	Tcte3	1.55	H2-Eb1	1.97	Usp18	2.91	Prmt2	-1.76	Chga	-1.22	Fbp1	-1.03
Nudt5	1.03	H2-M3	1.26	Trafd1	1.56	Cyp2d9	1.98	Lyz2	2.94	Fmo5	-1.75	Dgka	-1.22	Olfr165	-1.03
Klf7	1.04	Actn2	1.26	Lpcat2	1.56	Ctsw	1.99	Fcgr4	2.95	Slc5a6	-1.75	Rab3ip	-1.21	Cldn15	-1.02
Irf5	1.04	LOC100046959	1.27	Rhoj	1.56	Psmb8	1.99	Ifit2	2.96	Slc25a45	-1.73	Adam4	-1.21	Akr1e1	-1.02
LOC100045877	1.04	Myo1g	1.27	Lat	1.57	Cfp	1.99	Clec4d	2.97	Gprc5a	-1.73	Dgka	-1.21	A530082C11Rik	-1.02
Enpp4	1.05	Cyp3a13	1.27	Slc11a1	1.57	Samsn1	2	Ccl5	3.04	Dab1	-1.71	Klk1	-1.2	Samd9l	-1.02
2610200G18Rik	1.05	C1s	1.27	Samhd1	1.57	Stfa1	2.01	Gbp3	3.07	1300013J15Rik	-1.71	LOC670044	-1.2	Narf	-1.02
Slco2a1	1.05	D16Ertd472e	1.27	Wars	1.57	Cyp4f18	2.02	Cxcl13	3.15	LOC100044256	-1.7	Klk1b5	-1.2	Npc1l1	-1.02
Ly6e	1.05	Gm129	1.27	Rasgrp1	1.58	Rgs1	2.02	Serpina3g	3.19	Cps1	-1.7	Lamc2	-1.2	Als2	-1.02
4930570C03Rik	1.05	Tgm2	1.28	Ccl21a	1.59	Sult1a1	2.02	H2-Bl	3.22	Hmgcs2	-1.7	Dppa3	-1.2	Espn	-1.02
St6galnac6	1.05	Tbc1d10c	1.28	Lgmn	1.6	Tnfaip8l3	2.03	Serpina3n	3.25	Cyp2d26	-1.68	Cat	-1.19	As3mt	-1.02
Tha1	1.05	Prg2	1.28	Trat1	1.6	Akt3	2.04	Rac2	3.28	Aqp7	-1.67	2210023G05Rik	-1.19	Xpnpep2	-1.02
Nfkbib	1.05	Rbms1	1.29	H2-Ab1	1.6	A630077B13Rik	2.05	Lrg1	3.36	2010001J22Rik	-1.66	Sct	-1.19	Hist1h2bc	-1.01
Lst1	1.05	Zc3h12a	1.29	Flt1	1.6	Ccr5	2.05	Gbp2	3.38	Slc17a4	-1.65	Cyp4f16	-1.19	Uros	-1.01
Tapbpl	1.06	Evi2a	1.29	Mal	1.61	Sh2d2a	2.06	Il1b	3.38	Ptpro	-1.63	Gch1	-1.18	Adcy9	-1.01
Nod1	1.06	B3gnt7	1.29	Satb1	1.61	Slc11a1	2.06	Ccl4	3.39	Cyp2d26	-1.63	Reg1	-1.17	Krt7	-1.01
Cd160	1.06	Il15ra	1.3	EG667977	1.62	Cd68	2.06	Gpnmb	3.4	Faah	-1.61	2010110P09Rik	-1.17	Tfrc	-1.01
Nfkbiz	1.06	Unc93b1	1.3	Lck	1.62	Arhgdib	2.06	Hp	3.45	Cyp4v3	-1.61	Defa1	-1.16	Gpr89	-1
Nudt5	1.06	Fyb	1.3	Lpxn	1.62	Ifi47	2.07	Cd274	3.59	Snurf	-1.6	Anxa13	-1.16	2200002K05Rik	-1
Tlr7	1.07	Fbxo32	1.3	Cxcl4	1.62	Trim10	2.07	Hp	3.65	AY761184	-1.6	3110049J23Rik	-1.16	Ubfd1	-1
Lilrb4	1.07	LOC100046232	1.31	LOC667370	1.62	Ifit2	2.07	Serpina3f	3.78	Rragd	-1.6	Entpd5	-1.16	Pcdh24	-1
Tnfaip3	1.07	Gm129	1.31	Jdp2	1.63	1200002N14Rik	2.07	Chi3l3	3.81	Trpm4	-1.59	Slc6a4	-1.15	9530008L14Rik	-1
Mmp14	1.07	Tnfaip2	1.32	Gpr18	1.63	Nfkbia	2.08	Saa3	3.97	Sfrs7	-1.59	Vat1	-1.15		
Gimap7	1.07	Hoxb7	1.32	Itgb7	1.63	Gvin1	2.09	Cxcl10	3.99	Ugt2b35	-1.58	Ano7	-1.15		
Irgm1	1.08	Hcls1	1.32	9130218O11Rik	1.64	Nos2	2.09	Gbp2	4.03	Maob	-1.57	Pank1	-1.15		
Zap70	1.08	Ccdc88b	1.33	Il7r	1.64	Klhl6	2.12	Hp	4.17	2210417D09Rik	-1.57	Khk	-1.15		
ORF9	1.08	Cd40	1.33	Tlr13	1.64	Irgm1	2.13	Chi3l3	4.21	Dclk3	-1.56	Slc39a5	-1.15		
Cyp7b1	1.08	Aqp4	1.33	Ly6a	1.64	Icam1	2.13	Igtp	4.21	Tinag	-1.56	Slc23a2	-1.15		
Gns	1.09	Gpr65	1.34	Zap70	1.65	Slc15a3	2.13	Chi3l1	4.34	Dpep1	-1.54	Sprr2a	-1.15		
Slc11a1	1.09	Pstpip1	1.34	Coro1a	1.65	Erdr1	2.13	Ubd	4.49	St6galnac2	-1.53	Hace1	-1.14		
Rora	1.09	Clec4e	1.34	Nox1	1.65	Fut2	2.13	Cxcl9	4.53	LOC100047810	-1.53	Cdc42ep2	-1.14		
LOC100047934	1.09	Gpr114	1.34	Snx10	1.66	St6galnac6	2.14	Fpr2	4.67	Prlr	-1.52	Eno3	-1.14		
Msc	1.09	Fbxo32	1.34	Cd84	1.66	Laptm5	2.14	Chi3l3	5	9830002I17Rik	-1.51	Cisd1	-1.14		
Nrap	1.1	Rassf5	1.35	Rsad2	1.66	Tlr2	2.16	S100a9	5.42	Gjb3	-1.51	Clic6	-1.14		
Plekho2	1.1	Cd74	1.36	Plvap	1.66	Ms4a6d	2.16	Lcn2	5.89	Kalrn	-1.5	Adra2a	-1.14		
Sh3kbp1	1.1	H1fx	1.37	Unc93b1	1.67	E430002D04Rik	2.16	S100a8	6.14	Gstk1	-1.49	Prkcz	-1.14		
Fam110a	1.1	Pla2g2a	1.37	Siat7f	1.67	Mal	2.16	Pla2g4c	-6.08	Plek2	-1.48	Tmed1	-1.13		
LOC100045780	1.1	Pibf1	1.37	Fkbp5	1.67	Il1r2	2.17	LOC100045250	-5.22	Reg4	-1.48	Ggt1	-1.13		
Fas	1.11	D14Ertd668e	1.37	Cxcl2	1.68	Ccl17	2.17	AI987692	-5.04	Tppp	-1.48	Dpyd	-1.13		
Trafd1	1.12	Cdkn1c	1.37	Ccl21c	1.69	Lyzs	2.17	AI987692	-4.7	Slc39a5	-1.47	Ocm	-1.13		
Gpnmb	1.12	Ms4a7	1.38	Slc16a6	1.69	Ly6d	2.19	Mcm6	-4.13	Faah	-1.47	Acbd4	-1.12		
Nphp1	1.12	Dusp2	1.39	Mmp3	1.7	Coro1a	2.19	Abpb	-3.96	Sfn	-1.47	Mogat2	-1.12		
Itgae	1.12	Socs1	1.39	Aif1	1.71	Gcnt1	2.2	Gsdmc3	-3.96	Slc39a5	-1.46	Mogat2	-1.12		
Ets1	1.12	Ncf4	1.39	Ceacam12	1.71	Tac1	2.2	Arg2	-3.77	Uros	-1.46	Mboat1	-1.12		
Pira4	1.13	Cd14	1.4	Srgn	1.72	Cxcl1	2.21	LOC100043836	-3.72	Habp2	-1.46	Prap1	-1.12		
Ccbp2	1.13	Arrb2	1.4	Trim10	1.73	Ly6d	2.21	Tm4sf4	-3.41	Nts	-1.45	Prss23	-1.12		
Cd2	1.13	Prei4	1.4	Cd69	1.73	H2-M2	2.22	Ugt2b36	-3.25	Hbegf	-1.45	Acads	-1.11		
Vldlr	1.13	Napsa	1.4	Cytip	1.73	Cd177	2.23	Pdzk1	-3.03	Dnase1	-1.45	Klk1b4	-1.11		
Npm3	1.13	Areg	1.4	Irf1	1.74	Adh1	2.23	Fmo5	-2.94	Epb4.1l1	-1.43	Obfc1	-1.11		
Slc2a3	1.14	Msn	1.4	C1qa	1.74	Adh1	2.23	Pmp22	-2.92	Fam132a	-1.43	Upb1	-1.1		
2610524H06Rik	1.14	Tsc22d3	1.41	Saa1	1.74	Upp1	2.24	Ddc	-2.91	Gal3st2	-1.43	Ngef	-1.09		
Ifitm3	1.14	Wars	1.42	Sla	1.75	Fcgr3	2.27	Treh	-2.91	Thap4	-1.43	Ppap2a	-1.09		
Kcnab2	1.14	Tgtp	1.42	Gpx3	1.75	Gbp6	2.3	Rbp7	-2.85	Habp2	-1.42	Chgb	-1.09		
Fes	1.14	Pla2g7	1.42	Bcl2a1c	1.76	H2-Q8	2.3	Serpina1b	-2.65	Slc7a8	-1.42	Osbpl6	-1.09		
Csf1r	1.14	Adamtsl4	1.42	Ccl4	1.76	Ly6f	2.32	Ugt2b36	-2.59	Es1	-1.41	Klk1b27	-1.09		
Aif1	1.14	Lox	1.42	Srd5a2	1.76	Ly6c1	2.32	Asah2	-2.58	Ppfia3	-1.41	Pepd	-1.09		
LOC100041004	1.15	H2-Ab1	1.42	Clecsf9	1.76	LOC100044439	2.33	Abp1	-2.58	Defa1	-1.41	Cpa3	-1.09		
Usp2	1.15	Bcl2a1d	1.43	Arrdc4	1.76	Cp	2.35	Pnliprp2	-2.55	Mkks	-1.4	Rdm1	-1.09		
Irf1	1.15	Lcp1	1.43	EG630499	1.77	Igfbp3	2.35	Phlda2	-2.47	Rai14	-1.39	Abhd6	-1.09		
Gusb	1.15	Slfn1	1.44	Fcgr2b	1.77	Cd3g	2.36	Asah3	-2.44	Chga	-1.39	Acaa2	-1.08		
Arl6	1.15	Apob48r	1.44	Thy1	1.77	Fcgr2b	2.36	Cfl2	-2.42	Egln3	-1.37	Vkorc1	-1.08		
Il2rg	1.15	LOC100045005	1.44	Ctla4	1.78	Cd6	2.38	Pmp22	-2.4	Nrn1	-1.36	Cck	-1.08		
Hcst	1.15	P2ry13	1.45	0610010D20Rik	1.78	Cd52	2.38	Pnliprp2	-2.4	Hagh	-1.35	Chdh	-1.08		
Slc7a11	1.15	LOC641240	1.45	Irf1	1.79	Chac1	2.39	Cyp2d26	-2.39	2310005P05Rik	-1.35	Insig2	-1.08		
Tmc5	1.16	Gbp6	1.46	Clec7a	1.79	Clecsf12	2.4	Serpina1b	-2.37	Ces5	-1.34	Cmbl	-1.08		
Gimap6	1.16	Cpne8	1.47	BC051142	1.8	Emb	2.41	Mme	-2.31	Ppl	-1.34	5730472N09Rik	-1.08		
Cugbp2	1.16	Was	1.47	Dnase1l3	1.8	Apoe	2.41	Clps	-2.31	Epb4.1l1	-1.33	Gcg	-1.08		
BC026782	1.17	Ifitm6	1.47	Mmp3	1.8	Coro1a	2.42	Rdh7	-2.3	Hsd17b2	-1.33	Tmem139	-1.08		
Cd33	1.17	Lbp	1.47	Il1a	1.8	Ltf	2.45	Cyp2c67	-2.27	Tph1	-1.33	Bex4	-1.08		
Ildr1	1.17	Mmp3	1.47	Ifng	1.81	Usp18	2.45	Serpina1d	-2.27	Slco2b1	-1.32	1810020D17Rik	-1.07		
Tapbp	1.17	Ccr5	1.48	Tyrobp	1.81	Ifng	2.46	Clps	-2.26	Map3k6	-1.32	Galm	-1.07		
Gbp1	1.17	F10	1.48	Rgs1	1.81	Cd6	2.47	Lamb3	-2.25	Tm4sf5	-1.32	Tm6sf2	-1.07		
Sema6b	1.18	Icos	1.48	Klhl6	1.81	Ms4a6d	2.5	Igsf9	-2.23	Mmp15	-1.32	Atp2a3	-1.07		
Parp14	1.18	H2-DMa	1.48	Socs3	1.81	LOC100048461	2.51	Acsm3	-2.19	Ppfia3	-1.31	Sox21	-1.07		
Irf1	1.18	Scara3	1.48	Fxyd5	1.82	C1qc	2.52	Prlr	-2.16	Edn2	-1.31	Eva1	-1.07		

Table 5 – **Primers used in this study.**

qRT-PCR and PCR primers used in this study.
Murine Primers
TNFα forward: 5' - GCC TCC CTC TCA TCA GTT CT - 3'
TNFα reverse: 5' - CAC TTG GTG GTT TGC TAC GA - 3'
IFNγ forward: 5' - CAC GGC ACA GTC ATT GAA AG - 3'
IFNγ reverse: 5' - TTT TGC CAG TTC CTC CAG AT - 3'
IL-1β forward: 5’ - ACC TTT TGA CAG TGA TGA GAA – 3’
IL-1β reverse: 5’ - GAG ATT TGA AGC TGG ATG CT -3’
TLR2 forward: 5’ – GCT GGA GGA CTC CTA GGC T – 3’
TLR2 reverse: 5’ – GTC AGA AGG AAA CAH TCC GC – 3’
TLR4 forward: 5’ – ACC AGG AAG CTT GAA TCC CT – 3’
TLR4 reverse: 5’ – TCC AGC CAC TGA AGT TCT GA – 3’
PDGFRα forward: 5’ – TCC ATG CTA GAC TCA GAA GTC A – 3’
PDGFRα reverse: 5’ – TCC CGG TGG ACA CAA TTT TTC – 3’
SHH forward: 5’ – AAA GCT GAC CCC TTT AGC CTA – 3’
SHH reverse: 5’ – TTC GGA GTT TCT TGT GAT CTT CC – 3’
Wnt-5a forward: 5’ – CAA CTG GCA GGA CTT TCT CAA – 3’
Wnt-5a reverse: 5’ – CAT CTC CGA TGC CGG AAC T – 3’
GAPDH forward: 5’ – GGC AAA TTC AAC GGC ACA GT – 3’
GAPDH reverse: 5’ – AGA TGG TGA TGG GCT TCC C – 3’
Human Primers
PDGFRα forward: 5’ – TTT TTG TGA CGG TCT TGG AAG T -3’
PDGFRα reverse: 5’ – TGT CTG AGT GTG GTT GTA ATA GC -3’
Wnt-5a forward: 5’ – TCG ACT ATG GCT ACC GCT TTG – 3’
Wnt-5a reverse: 5’ – CAC TCT CGT AGG AGC CCT TG – 3’
GAPDH forward: 5’ – TTC TAT AAA TTG AGC CCG CA - 3’
GAPDH reverse: 5’ – CGA CGC AAA AGA AGA TGC - 3’
16S Primers
338F: 5′ - GTGCCAGCMGCCGCGGTAA - 3′
806R: 5′ - GGACTACHVGGGTWTCTAAT - 3′